Revista Mexicana de Astronomía y Astrofísica, **33**, 31–57 (1997)

WEAK RADIO GALAXIES. I. BROAD-BAND OPTICAL IMAGING

R. Carrillo and I. Cruz-González

Instituto de Astronomía
Universidad Nacional Autónoma de México

and

J. Guichard

Instituto Nacional de Astrofísica, Optica y Electrónica
Tonantzintla, Pue., México

Received 1996 July 1; accepted 1997 February 10

RESUMEN

Reportamos un estudio de las propiedades ópticas de radiogalaxias débiles (WRGs) del catálogo V2, para obtener las propiedades fotométricas de banda ancha e información morfológica crucial para nuestras imágenes de banda angosta en Hα y [O III] (Carrillo et al. 1997). Este trabajo contiene imágenes ópticas CCD de 30 radiogalaxias débiles obtenidas en *V, R* e *I*. Presentamos los resultados morfológicos y fotométricos de las WRGs y se discuten su relaciones con la radio estructura y el medio ambiente en el que están inmersas. Encontramos que la mayoría de las WRGs son elípticas, tienen morfologías peculiares y se encuentran en ambientes de alta densidad de galaxias. Los colores ópticos de las WRGs son peculiares si se comparan con colores de galaxias elípticas normales pero similares a los colores de los AGNs. Los perfiles de brillo superficial de la mayoría de las WRGs siguen la esperada ley de de Vaucouleurs para elípticas en la mayoría de los radio, pero en todos los casos se observa una caída o aplanamiento en las porciones más internas de los perfiles, probablemente producido por una fuente de emisión nuclear adicional. Los efectos de mareas producidos por galaxias compañeras descritos por Kormendy (1977) para elípticas, son claramente evidentes en las porciones externas de los perfiles de las WRGs y pueden ser asociados a efectos de interacción.

ABSTRACT

We report on a study of the optical properties of weak radio galaxies (WRGs) from the B2 survey, to obtain the broad-band photometric properties and morphology information crucial for our narrow-band imaging at Hα and [O III] study (Carrillo et al. 1997). This paper contains optical CCD images of 30 radio galaxies obtained at *V, R* and *I*. We present the morphological and photometric results and discuss their relationship to the radio structure and environmental properties. We find that most WRGs are E galaxies, have peculiar morphologies and are located in high galaxy density environments. Optical colors of WRGs are unusual if compared to colors of normal ellipticals, but similar to AGN colors. The surface brightness profiles of most WRGs follow the de Vaucouleurs law expected for ellipticals at most radii, but in all cases a turnover or flatness is observed in the innermost portion of the profiles, possibly produced by an additional nuclear emission source. The tidal effects produced by galaxy companions described by Kormendy (1977) for ellipticals, are clearly evident in the outer parts of the WRGs profiles and can be associated to interaction effects.

Key words **GALAXIES – ACTIVE — GALAXIES – INTERACTIONS — GALAXIES – NUCLEI — GALAXIES – PHOTOMETRY**

1. INTRODUCTION

This is the first in a series of papers discussing optical and infrared properties in low luminosity radio galaxies ($P_{1.4\ GHz} < 10^{24.5}$ W Hz^{-1}) with FRI radio morphologies (Fanaroff & Riley 1974). We have obtained optical images of 30 radio sources selected from the second Bologna survey (B2). The images obtained include broad-band data at V, R, and I, presented here, narrow-band data at Hα and [O III] at the corresponding galaxy redshifts presented in Carrillo (1995) and Carrillo et al. (1997), and J, H, and K data presented in Cruz-González, Carrillo, & Salas (1997).

Although early type galaxies are known to be poor in cool gas, the discovery of near-nuclear extended, and very extended line-emitting gas (e.g., Baum et al. 1988) in E and S0 galaxies is quite puzzling. The origin of the extended emission line nebulae (EELNs) at distances of several kpc of the nuclei of radio galaxies, may suggest that the gas has been acquired during interactions with a gas rich companion. The manifestations of such interactions should be observable in the optical. In fact, Smith & Heckman (1989a) study of powerful radio galaxies (PRGs) showed that more than half of their sources have morphological distortions and unusual colors probably due to interactions with galaxy companions. Another possibility, is that the emission line gas is the product of the intracluster environmental gas, but the statistical estimates are still quite uncertain. In PRGs the presence of extended emission-line gas is quite common as is shown by Baum & Heckman (1989a, 1989b). These authors found that in a sample of powerful radio sources ($P_{1.4\ GHz} > 10^{24.5}$ W Hz^{-1}) with FRII radio morphologies, 85% of the galaxies have resolved line-emitting regions, with a variety of morphologies: some sources are small, centrally condensed and roughly symmetric about the host galaxy nuclei, often with roughly "oval" or "elliptical shapes" while in other, there are extended filaments at tens of kpc from the host galaxy nucleus. González-Serrano & Carballo (1993), studied a sample of 24 low-luminosity radio galaxies (B2) with observed radio jets; 7 of these galaxies are also studied in our paper. These authors show that a high fraction (75%) of their objects have morphological peculiarities that can be associated with indicators of other recent merger processes or gravitational interaction. These authors and Heckman et al. (1986), argue that the difference between FRII and FRI sources is that the first interact with gas-rich systems, while the latter interact with gas-poor galaxies, and that the host galaxies of low-luminosity radio sources with jets could form cD galaxies.

The principal goals in our study of low-luminosity or weak radio galaxies (WRGs) are the understanding of the following questions: (1) what is the morphology of the weak radio galaxies? (2) are the host galaxies normal E galaxies or do they have abnormalities? (3) what is the origin of the peculiarities in WRGs: collisions, merging or interaction with ambiental cool gas? (4) if interactions occur, what are the morphological types of the galaxies involved? (5) what is the fraction of WRGs with abnormal morphology and how does it compare to powerful radio galaxies? and, (6) what is the effect of the possible interactions in the morphological properties of the extended radio sources?

In this paper we present the broad-band optical images, photometric and morphological properties. The paper is organized as follows: In § 2 a description of the observations and sample is presented, the image analysis procedures are described in § 3, the photometric and morphological results are in § 4, followed by a discussion of the WRG properties found in § 5. An individual galaxy description is presented in § 6, and a summary of results and conclusions are in § 7.

2. OBSERVATIONS

2.1. Sample Selection

The observed sample consists of 30 galaxies identified with the radio sources of the Second Bologna Survey (B2). This survey is divided into two groups: the bright sample, complete to limiting magnitudes $m_{pg} = 15.7$ (Fanti et al. 1973; Colla et al. 1975a, 1975b), and the faint sample, complete to $m_V = 16.5$ (Fanti et al. 1978). The first group is associated with galaxies in the Zwicky Catalogue, while the second is identified with galaxies in the POSS plates. The B2 sample is defined by $S_{408\ MHz} > 0.25$ Jy and $+24° < \delta < +34°$ (Colla et al. 1973). The complete sample has been studied at 1.4 GHz with different configurations of the VLA (Parma et al. 1986; de Ruiter et al. 1986; Fanti et al. 1987). The radio studies provided information about radio galaxy luminosities, morphological properties (Fanti et al. 1987; Parma et al. 1987), jet properties (Parma et al. 1987), and polarization (Morganti et al. 1987; Capetti et al. 1993).

Photometric images of 30 weak radio galaxies are presented in this paper. Two selection criteria were adopted, all galaxies are members of the B2 survey with low redshifts ($z \leq 0.07$), and most of them have a core and jet radio structure with radio powers $P_{1.4\ GHz} < 10^{24.5}$ W Hz^{-1} (i.e., they are all type FRI). The source 1318+34, which has an uncertain B2 identification (Fanti et al. 1987), was included due to its interesting peculiar optical morphology.

The characteristics of the WRGs studied here are presented in Table 1: col. 1, B2 source; col. 2, other names; col. 3, redshift; col. 4 and col. 5, coordinates; col. 6, visual or photographic magnitude; col. 7,

galaxy morphological type; col. 8, radio source type (B2 Survey): bright (B), faint (F); col. 9, comments.

2.2. Instrumentation

The observations were carried out at the 2.1-m telescope of the Observatorio Astronómico Nacional at San Pedro Mártir (OAN/SPM), B.C., México, during several observing runs: April and September 91; March, June, July, September and October 92; April and September 93. CCD images were taken through the following broad-band filters: Johnson V and Kron-Cousins R and I.

Two Thompson CCD detectors were used: 384 × 576 and 1024 × 1024, which —with the f/7.5 secondary— yield an image scale in the focal plane of 0.3″/pixel and 0.25″/pixel, respectively. Thus the fields of view are 1.93′× 2.89′ and 4.25′×4.25′, in each case. The CCD detector properties are: Th384 × 576, 11 e^{-1} read-out noise and 23 μm pixel size; Th1024 × 1024, 5.73 e^{-1} read-out noise and 19 μm pixel size.

TABLE 1

SAMPLE OF B2 RADIO GALAXIES

Source B2 (1)	Other Name (2)	z (3)	α (1950) (4)	δ (5)	m (6)	Morph. Type (7)	Type B2 (8)	Comments (9)
0034+25	...	0.0321	00 34 26.8	25 25 26	14.80[a]	...	B	...
0055+26	NGC 326	0.0472	00 55 40.7	26 35 44	12.50[a]	D	B	group of gal.
0116+31	4C31.04	0.0592	01 16 47.1	31 55 07	15.70[a]	DB	B	group of gal.
0120+33	NGC 507	0.0164	01 20 50.7	32 59 45	13.00[a]	E	B	group of gal.
0206+35	4C 35.03	0.0375	02 06 39.3	35 33 41	14.90[a]	D	B	...
0331+39	4C 39.12	0.0202	03 31 01.0	39 11 25	14.20[a]	E	B	...
0838+32	4C 32.26	0.0680	08 38 06.8	32 35 39	14.80[b]	E2	F	pair of gal.
0913+38	...	0.0711	09 13 39.1	38 30 41	15.70[b]	...	F	...
0916+33	...	0.0500	09 16 50.1	33 07 54	15.70[a]	Sc	B	...
1108+27		0.0331	11 08 43.4	27 14 06	14.60[a]	E	B	...
1116+28	...	0.0667	11 16 19.1	28 10 32	14.30[b]	...	F	...
1122+39	NGC 3665	0.0067	11 22 01.4	39 02 19	11.60[a]	E2	B	...
1217+29	NGC 4278	0.0021	12 17 36.6	29 33 29	11.20[a]	E	B	BLRG
1318+34[c]	...	0.0232	13 18 16.9	34 23 56	14.80[a]	...	B	peculiar gal.
1322+36	NGC 5141	0.0175	13 22 35.4	36 38 19	13.90[a]	D	B	...
1339+26	4C 26.41	0.0688	13 39 30.7	26 37 20	14.20[b]	SE	F	...
1346+26	4C 26.42	0.0633	13 46 35.0	26 50 30	15.50[a]	CD	B	Abell 1795
1357+28	...	0.0629	13 57 45.2	28 44 28	14.60[b]	...	F	...
1422+26	...	0.0370	14 22 26.5	26 51 26	15.60[a]	E2	B	...
1441+26	...	0.0621	14 41 53.9	26 13 51	14.30[b]	...	F	...
1557+26	...	0.0442	15 57 45.9	26 04 51	14.30[b]	...	F	...
1652+39	4C 39.49	0.0337	16 52 11.8	39 50 25	13.70[a]	N	B	Mk 501
1658+30	4C 30.31	0.0351	16 58 48.9	30 12 32	15.10[b]	...	F	pair of gal.
1752+32	...	0.0449	17 52 44.5	32 34 45	14.30[b]	...	F	...
1833+32	3C 382	0.0586	18 33 12.0	32 39 18	15.50[a]	D3	B	BLRG
1855+37	...	0.0552	18 55 54.3	37 56 27	14.90[a]	...	B	group of gal.
2116+26	...	0.0164	21 16 20.7	26 14 08	14.00[a]	E	B	...
2236+35	...	0.0277	22 36 12.3	35 04 11	15.00[a]	E	B	group of gal.
2320+32	...	0.0177	23 20 43.4	32 15 09	14.50[a]	S	B	...
2335+25	NGC 7720	0.0301	23 35 59.0	26 45 15	13.90[a]	D	B	Abell 2634

[a] Photographic magnitude.
[b] Visual magnitude.
[c] Source with uncertain identification.

TABLE 2

STANDARD STARS

Date of Observation (1)	Standard Stars (2)
Apr. 1991	99-340, 99-438, 105-447, 105-448, 109-231
Sep. 1991	109-1082, 111-2864, 115-349
Mar. 1992	96-405, 96-406, 97-346
Jun. 1992	104-305, 104-306
Jul. 1992	104-461, 106-485
Sep. 1992	114-473
Oct. 1992	114-473
Apr. 1993	101-24
Sep. 1993	92-336, 111-773, 111-775

2.3. Photometric Observations

A set of standard stars from Landoldt (1983) were acquired each night for the photometric calibration. The standard star observations are presented in Table 2, which contains the date of observation and the list of standards for each observing run.

The details of the galaxy observations are presented in Table 3. The contents are the following: col. 1, source name; col. 2, date of observation; col. 3, filter; col. 4, integration time; col. 5, FWHM of PSF. Most galaxies were observed with all the filters during the same observing run and some galaxies were observed in two different runs for calibration purposes. The typical seeing during our observations was in the range 1.0 to 2.2″.

3. IMAGE ANALYSIS

The reduction of the two-dimensional CCD frames follows the standard procedures (e.g., Kent 1984; Cornell et al. 1987). The NOAO Image Reduction and Analysis Facility (IRAF) software package was used. The adopted reduction procedure was the following:

1. To remove the detector response, each image is bias subtracted, using a mean of 9 bias frames, and then divided by the mean of at least 4 flat field sky exposures obtained at twilight.

2. The sky background is determined in each frame to first approximation by constructing a count frequency histogram and estimating the intensity level corresponding to the maximum frequency.

3. Accurate determination of object centroids is performed, by fitting a Gaussian bidimensional profile to the data, centered on the brightest excess in each object, generally corresponding to the galaxy nucleus. To partly remove residual misalignments in the regions where light gradients are more pronounced, the images were smoothed using Gaussian filters of 2 pixels FWHM.

4. Direct inspection to the frames allowed removal of cosmic rays and bad pixels.

5. The galaxy images were calibrated using the faintest $UBVRI$ standards of Landolt 1983. The images R and I from the Kron-Cousins system were transformed to the Johnson system. The colors $(V-R)$, $(R-I)$ and $(V-I)$ for the galaxies, were obtained using the extinction coefficients for OAN/SPM of Schuster (1982). The extinction (A_V) was obtained from Savage & Mathis (1979) and the redshift correction $(K_V(z))$ was obtained using the formulas of Whitford (1971). The color transformation equations for the two CCDs used are presented in Carrillo & Martínez (1997).

6. The WRGs images and magnitudes presented in this paper correspond to the final image obtained at each filter. This final image is the combined image of at least 4 frames obtained at each filter.

7. V, R, and I magnitudes are derived by integrating the light profiles up to the radius that corresponds to the 25 mag/arcsec^2 isophote. The magnitudes are measured quantities and are not corrected to the face-on values.

8. V, R, and I profiles are derived for 30 weak radio galaxies. These profiles correspond to the final combined image.

4. PHOTOMETRIC AND MORPHOLOGICAL RESULTS

4.1. Images

The final images of the WRGs studied in this paper, are presented in Figures 1*a* to 1*d*. For brevity, only R filter images are presented for each galaxy, with the orientation north up and east to the left, but V and I images are available upon request. The bars in these images correspond to 15″. Of the 30 radio galaxies studied, we have photometric quality images at V, R, and I for 27 WRGs and only at R and I for the remaining 3.

These images show that several galaxies are very elliptical in appearance, others are pairs (usually E+E) with comparable intensities and a common halo, few are in groups of galaxies of different intensities and the rest show small components fainter than the dominant nucleus (hot spots) in a common halo.

Contour maps of radio galaxies at I are shown in Figures 2*a* to 2*d*. The convention used for the multiple component systems is as follows: galaxies with companions are indicated by capital letters; A, is the brighter and the rest are labelled in decreasing intensity (B, C, ...); galaxies with hot spots, i.e., small components of low surface brightness, are labelled with lower case letters (a, b, ...) in order of decreasing brightness (cf., Figure 1*a* to 1*d* and Table 4, col. 2.

TABLE 3

OBSERVATIONS

Source Name (1)	Date of Observ. (2)	Filter (3)	Int. Time (sec) (4)	FWHM of PSF (″) (5)	Source Name (1)	Date of Obser. (2)	Filter (3)	Int. Time (sec) (4)	FWHM of PSF (″) (5)
0034+25	93 Sep[a]	*V*	30	1.5	1339+26	93 Apr[a]	*V*	300	1.6
		R	20	1.3		92 Mar[a]	*R*	600	1.7
		I	20	1.4			*I*	600	1.3
0055+26	92 Oct[a]	*V*	180	1.4	1346+26	93 Apr[a]	*V*	120	2.0
		R	20	1.6		92 Mar[a]	*R*	120	1.7
		I	20	1.4			*I*	120	1.2
0116+31	92 Oct[a]	*V*	240	1.4	1357+28	93 Apr[a]	*V*	600	1.6
		R	180	1.3		91 Apr[b]	*R*	600	2.0
		I	180	1.5			*I*	600	2.1
0120+33	93 Sep[a]	*V*	600	1.9	1422+26	92 Jun[a]	*R*	300	2.0
		R	480	2.2			*I*	300	2.0
		I	300	2.2	1441+26	91 Apr[b]	*V*	600	1.9
0206+35	93 Sep[a]	*V*	600	1.5			*R*	600	1.9
		R	300	1.6			*I*	600	1.6
		I	180	1.5	1557+26	92 Jul[a]	*V*	180	1.4
0331+39	93 Sep[a]	*V*	300	1.4			*R*	300	1.3
		R	300	1.4			*I*	240	1.4
		I	300	1.5	1652+39	93 Apr[a]	*V*	180	1.3
0838+32	91 Apr[b]	*V*	600	1.8		92 Mar[a]	*R*	120	1.7
		R	600	2.1			*I*	60	1.4
		I	600	1.8	1658+30	93 Apr[a]	*V*	300	1.8
0913+38	92 Mar[a]	*V*	600	1.7		92 Jun[a]	*R*	300	2.2
		R	600	1.5			*I*	300	2.2
		I	600	1.1	1752+32	91 Sep[b]	*V*	600	2.1
0916+33	92 Oct[a]	*V*	600	1.8			*R*	600	2.1
		R	300	1.5			*I*	600	2.2
		I	480	1.8	1833+32	91 Sep[b]	*V*	600	2.0
1108+27	91 Apr[b]	*V*	600	1.9			*R*	600	2.2
		R	600	2.2			*I*	600	1.9
		I	600	2.0	1855+37	91 Sep[b]	*V*	600	2.0
1116+28	92 Mar[a]	*V*	600	1.2			*R*	600	2.1
		R	300	1.3			*I*	600	1.9
		I	120	1.0	2116+26	92 Oct[a]	*V*	45	1.6
1122+39	91 Apr[b]	*V*	600	2.4			*R*	40	1.6
		R	600	1.8			*I*	30	1.7
		I	600	2.2	2236+35	93 Sep[a]	*V*	240	1.7
1217+29	91 Apr[b]	*V*	600	2.2			*R*	300	1.6
		R	600	1.7			*I*	120	1.5
		I	150	1.5	2320+32	91 Sep[b]	*V*	600	2.1
1318+34	91 Apr[b]	*R*	600	1.8			*R*	600	1.9
		I	600	1.6			*I*	600	2.0
1322+36	91 Apr[b]	*R*	600	1.8	2335+26	91 Sep[b]	*V*	600	2.1
		I	600	1.6			*R*	600	2.1
		I	600	1.6			*I*	600	2.0

[a] Size of CCD: 1024 × 1024 pixel.
[b] Size of CCD: 384 × 576 pixel.

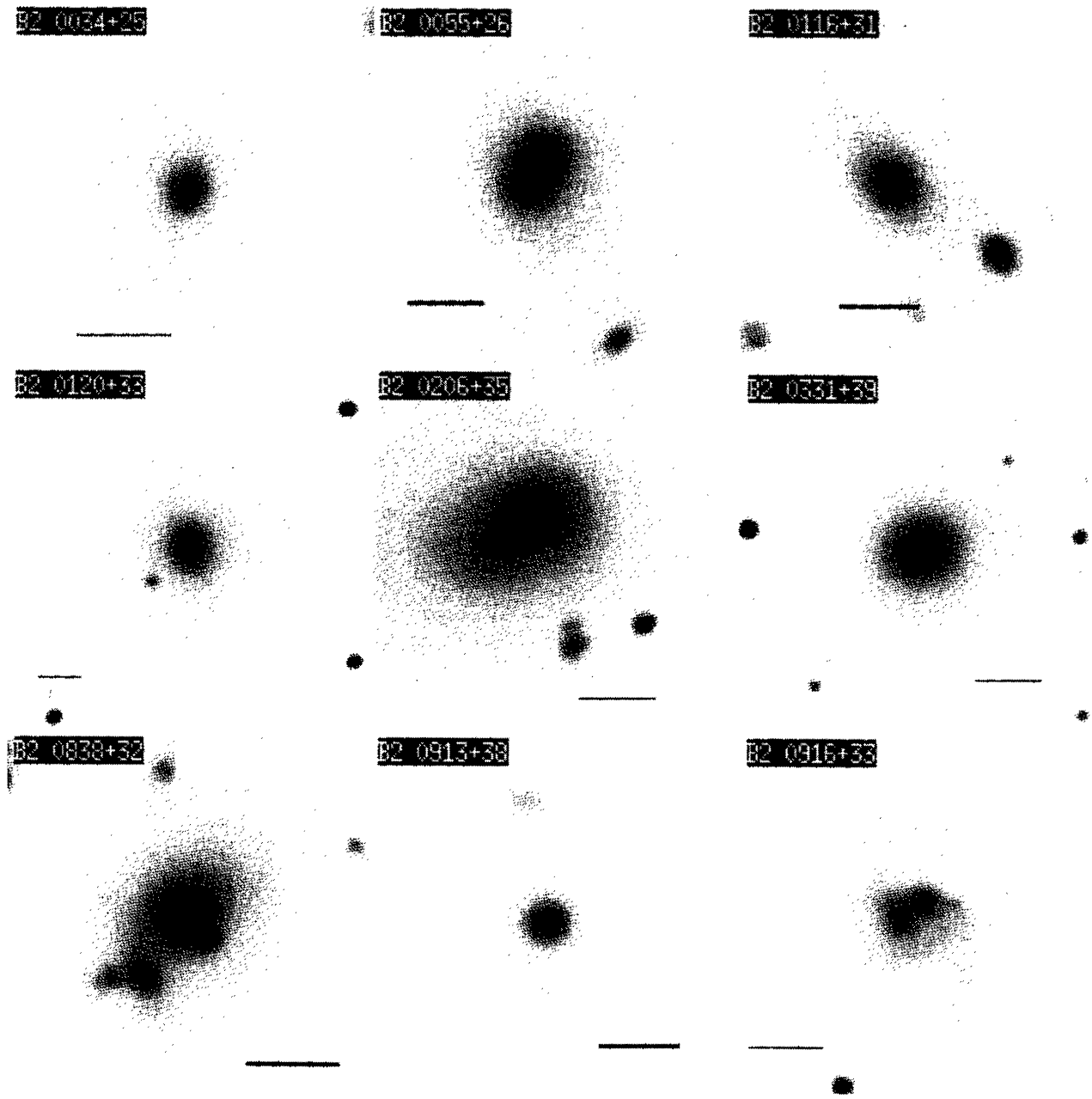

Fig. 1*a*. CCD images of 30 B2 radio galaxies at R filter. In these maps, north is up and east is left. The bar corresponds to 15″.

4.2. Photometry and Geometry

The photometric results and geometrical parameters derived for the WRGs studied in this paper, are given in Table 4 and Table 5. These parameters were obtained using several routines in the IRAF package: isophote (ellipse) in STSDAS, apphot in DIGIPHOT (phot, polyphot, fitskypars, etc.). The following quantities were obtained for each galaxy:

1. Total apparent magnitude in V, R, and I are calculated with estimated photometric errors of 3–5%. If there were multiple components in a common halo the magnitude corresponds to all the components. Apparent magnitudes at R and $(V-R)$ and $(R-I)$ colors are given (cf., Table 4, cols. 2 to 4).
2. Ellipticity of the best fitting ellipse with a 25 mag/arcsec^2 limit. The e's are observed values, i.e.,

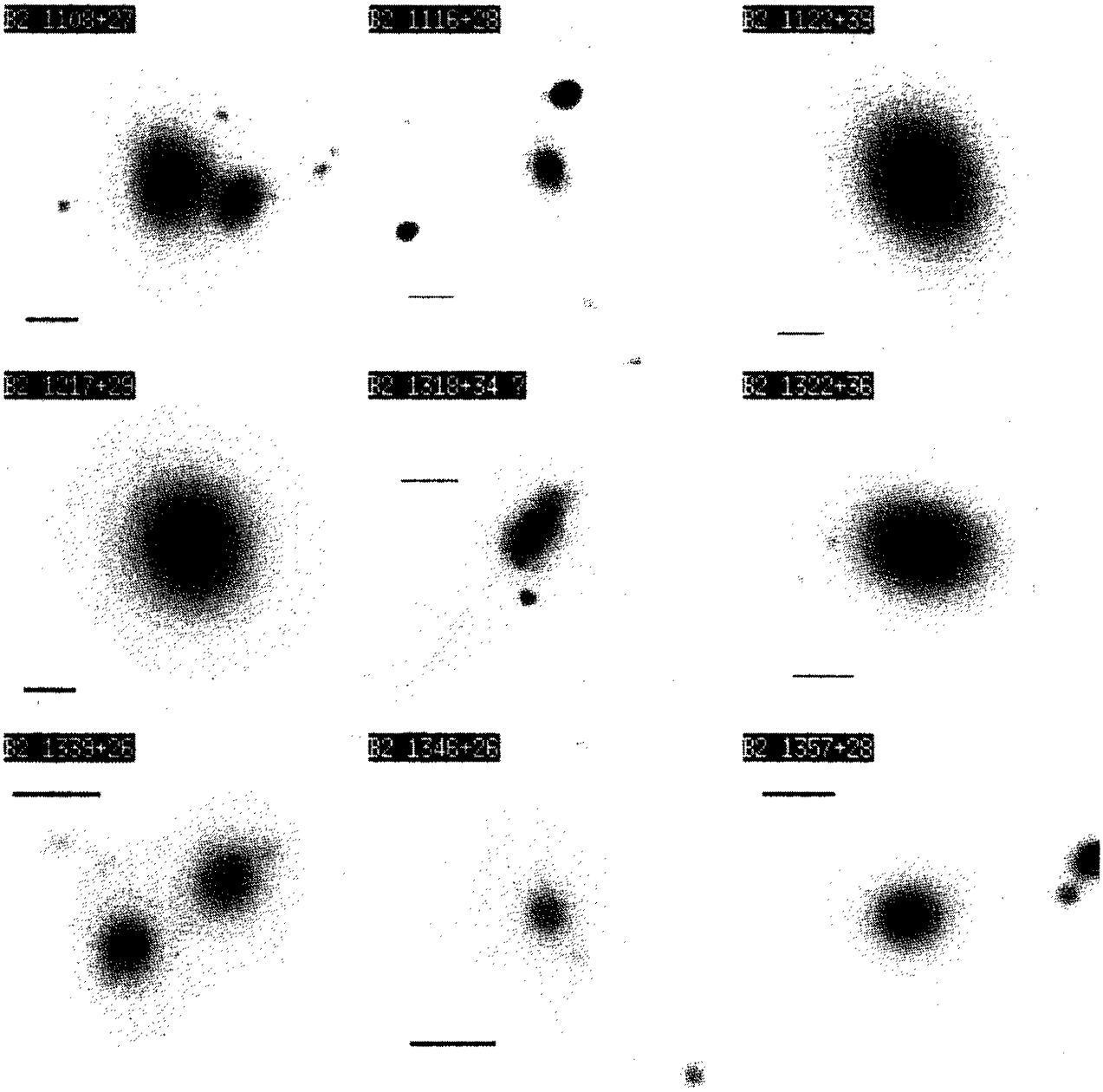

Fig. 1*b*. Same as Figure 1*a*.

no face-on corrections were applied. If there were multiple components, each component in a galaxy field is fitted and estimated errors are given (cf., Table 5, col. 1).

3. Position angles in degrees of the best fitting ellipse that correspond to the major axis, the values of the P.A.s follow the usual convention (cf., Table 5, col. 2). The P.A.s are observed values, i.e., no face-on correction were applied.

4.3. Light Profiles

The surface brightness profiles of each galaxy were obtained using several routines in the STSDAS subroutines of IRAF. They were obtained from the ellipsoidal fits to the I images (previously convolved with a Gaussian of 2 pixels FWHM). The profiles are obtained from the intensity at different positions along the major axis of the ellipse. We note that the

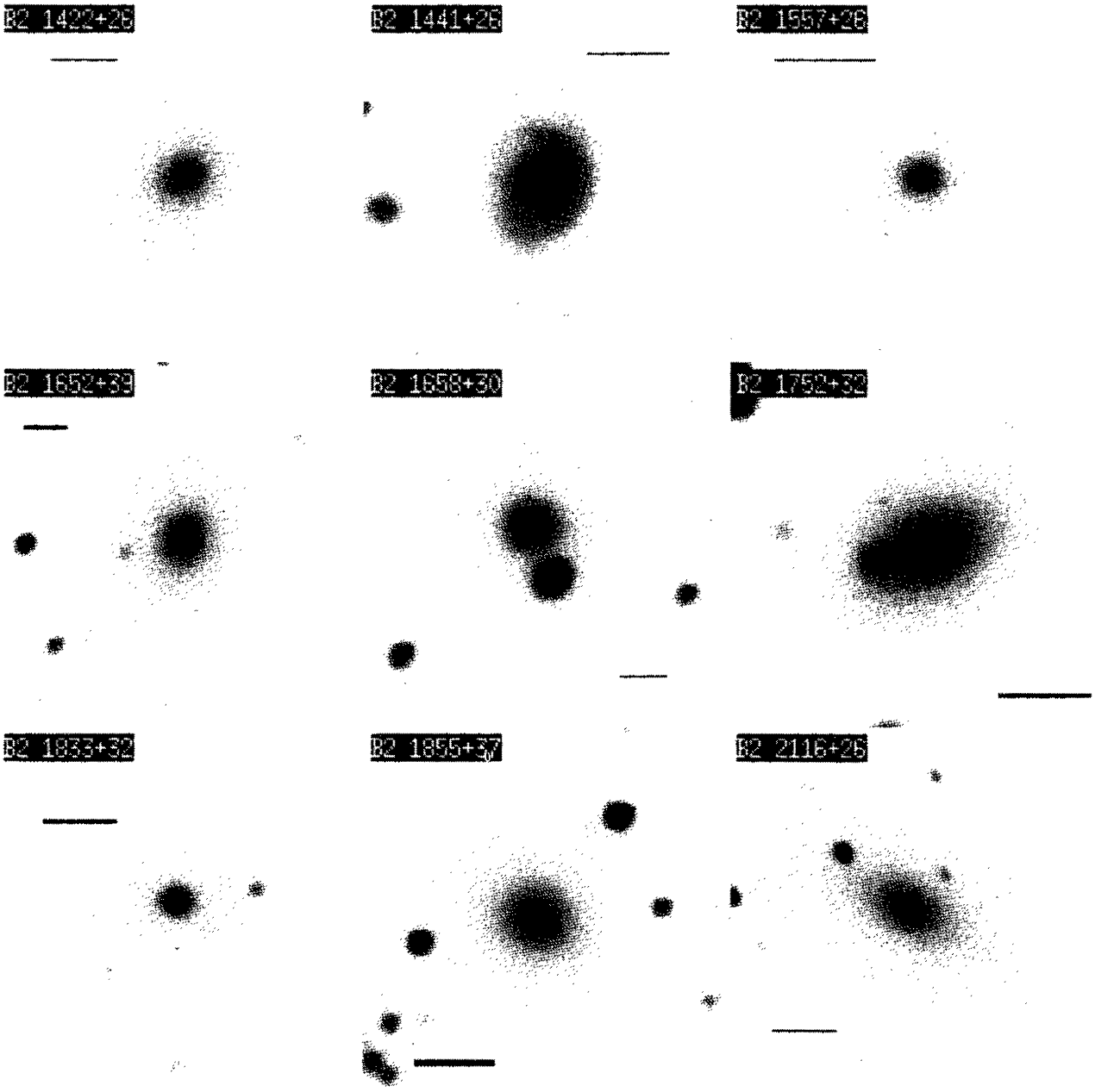

Fig. 1*c*. Same as Figure 1*a*.

profiles obtained at R and I show no significant differences, but this would be further studied once the near infrared analysis is completed.

In Figures 3*a* to 3*h*, we present the WRGs surface brightness profiles, observed μ (mag/arcsec^2) versus the fourth root of the major axis, a$^{1/4}$ (arcsec$^{1/4}$).

5. DISCUSSION

5.1. Optical Morphology

A direct inspection of the broad-band images presented in Fig. 1*a* to 1*d* and the contour maps in Fig. 2*a* to 2*d* of the WRGs studied here, show that sev-

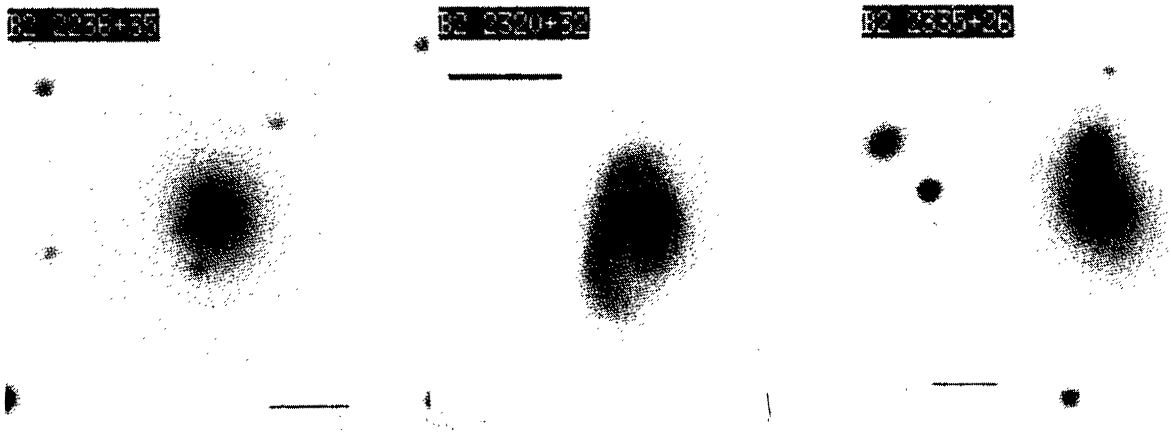

Fig. 1*d*. Same as Figure 1*a*.

TABLE 4

PHOTOMETRIC RESULTS

Source B2 (1)	R (mag) (2)	$(V-R)$ (mag) (3)	$(R-I)$ (mag) (4)	Source B2 (1)	R (mag) (2)	$(V-R)$ (mag) (3)	$(R-I)$ (mag) (4)
0034+25	13.37	0.63	0.65	1339+26	12.98	1.11	0.41
	±0.04	±0.01	±0.01		±0.01	±0.01	±0.01
0055+26	12.93	0.77	0.71	1346+26	13.43	1.10	0.15
	±0.01	±0.01	±0.01		±0.02	±0.04	±0.04
0116+31	13.73	0.64	0.69	1357+28	14.35	0.31	0.58
	±0.01	±0.02	±0.02		±0.02	±0.04	±0.04
0120+33	11.67	0.91	0.93	1422+26	13.86	...	0.56
	±0.02	±0.04	±0.04		±0.01	...	±0.02
0206+35	12.91	0.65	0.68	1441+26	14.20	0.45	0.63
	±0.01	±0.04	±0.03		±0.04	±0.04	±0.06
0331+39	12.66	0.70	1.00	1557+26	14.17	0.55	0.82
	±0.01	±0.01	±0.01		±0.03	±0.04	±0.05
0838+32	14.00	0.61	1.01	1652+39	12.61	1.01	0.83
	±0.01	±0.02	±0.02		±0.02	±0.04	±0.04
0913+38	15.21	0.41	0.79	1658+30	13.13	1.59	0.44
	±0.01	±0.01	±0.01		±0.04	±0.03	±0.03
0916+33	15.02	−0.90	1.46	1752+32	14.68	−0.34	1.58
	±0.01	±0.01	±0.01		±0.01	±0.01	±0.01
1108+27	12.79	0.43	0.58	1833+32	13.69	0.77	0.42
	±0.01	±0.01	±0.01		±0.03	±0.05	±0.05
1116+28	14.75	−0.90	1.75	1855+37	13.55	0.34	0.74
	±0.01	±0.02	±0.02		±0.01	±0.01	±0.01
1122+39	10.55	0.47	−0.24	2116+26	12.92	0.52	0.94
	±0.01	±0.01	±0.01		±0.03	±0.01	±0.01
1217+29	10.04	0.54	0.51	2236+35	13.72	0.65	0.68
	±0.01	±0.01	±0.01		±0.03	±0.01	±0.01
1318+34	14.49	...	0.38	2320+32	13.69	0.52	0.45
	±0.02	...	±0.04		±0.02	±0.04	±0.04
1322+36	12.37	...	0.98	2335+26	12.72	0.73	0.67
	±0.01	...	±0.01		±0.01	±0.01	±0.01

TABLE 5

POSITION ANGLES AND ELLIPTICITY

Source B2 (1)	e (2)	PA (°) (3)	Source B2 (1)	e (2)	PA (°) (3)
0034+25	0.07 ± 0.01	158 ± 0	1322+36	0.12 ± 0.00	66 ± 1
0055+26A	0.07 ± 0.02	115 ± 8	1339+26A	0.06 ± 0.02	149 ± 3
0055+26B	0.04 ± 0.01	108 ± 3	1339+26B	0.08 ± 0.01	129 ± 3
0116+31	0.15 ± 0.01	38 ± 2	1346+26	0.07 ± 0.04	51 ± 2
0120+33	0.02 ± 0.02	9 ± 0	1357+28	0.08 ± 0.03	110 ± 4
0206+35	0.08 ± 0.01	128 ± 6	1422+26	0.17 ± 0.05	136 ± 5
0331+39	0.08 ± 0.01	118 ± 3	1441+26	0.06 ± 0.07	36 ± 9
0838+32A	0 .13 ± 0.02	134 ± 12	1557+26	0.07 ± 0.04	89 ± 2
0838+32B	0 .27 ± 0.01	44 ± 9	1652+39	0.12 ± 0.02	131 ± 1
0838+32a	0.21 ± 0.01	46 ± 10	1658+30A	0.15 ± 0.03	138 ± 1
0838+32b	0.26 ± 0.02	49 ± 7	1658+30B	0.07 ± 0.02	135 ± 1
0913+38	0.08 ± 0.01	33 ± 8	1752+32A	0.11 ± 0.02	90 ± 4
0916+33A	0.05 ± 0.018	36 ± 8	1752+32B	0.13 ± 0.01	83 ± 11
0916+33B	0.06 ± 0.02	166 ± 0	1833+32	0.09 ± 0.04	89 ± 11
1108+27A	0.06 ± 0.03	178 ± 3	1855+37	0.05 ± 0.02	58 ± 7
1108+27B	0.08 ± 0.04	111 ± 7	2116+26	0.07 ± 0.01	63 ± 10
1116+28	0.09 ± 0.00	14 ± 7	2236+35A	0.06 ± 0.01	166 ± 9
1122+39	0.11 ± 0.03	32 ± 3	2236+35a	0.22 ± 0.05	110 ± 6
1217+29A	0.06 ± 0.01	37 ± 15	2236+35b	0.13 ± 0.02	118 ± 5
1217+29a	0.15 ± 0.06	63 ± 7	2320+32	0.15 ± 0.02	108 ± 6
1318+34A	0.13 ± 0.03	157 ± 2	2335+26A	0.03 ± 0.02	22 ± 4
1318+34a	0.07 ± 0.02	37 ± 9	2335+26B	0.05 ± 0.02	135 ± 18

eral galaxies, about 63%, have clear morphological peculiarities. In Table 6, col. 2, we present the morphological description of each galaxy in our sample. We have followed the terminology presented by Heckman et al. (1986), and Smith & Heckman (1989a, 1989b): NE = normal E galaxies and ND = normal disk galaxies with no apparent peculiarities, B = bridge between galaxy and a companion, CE = radio

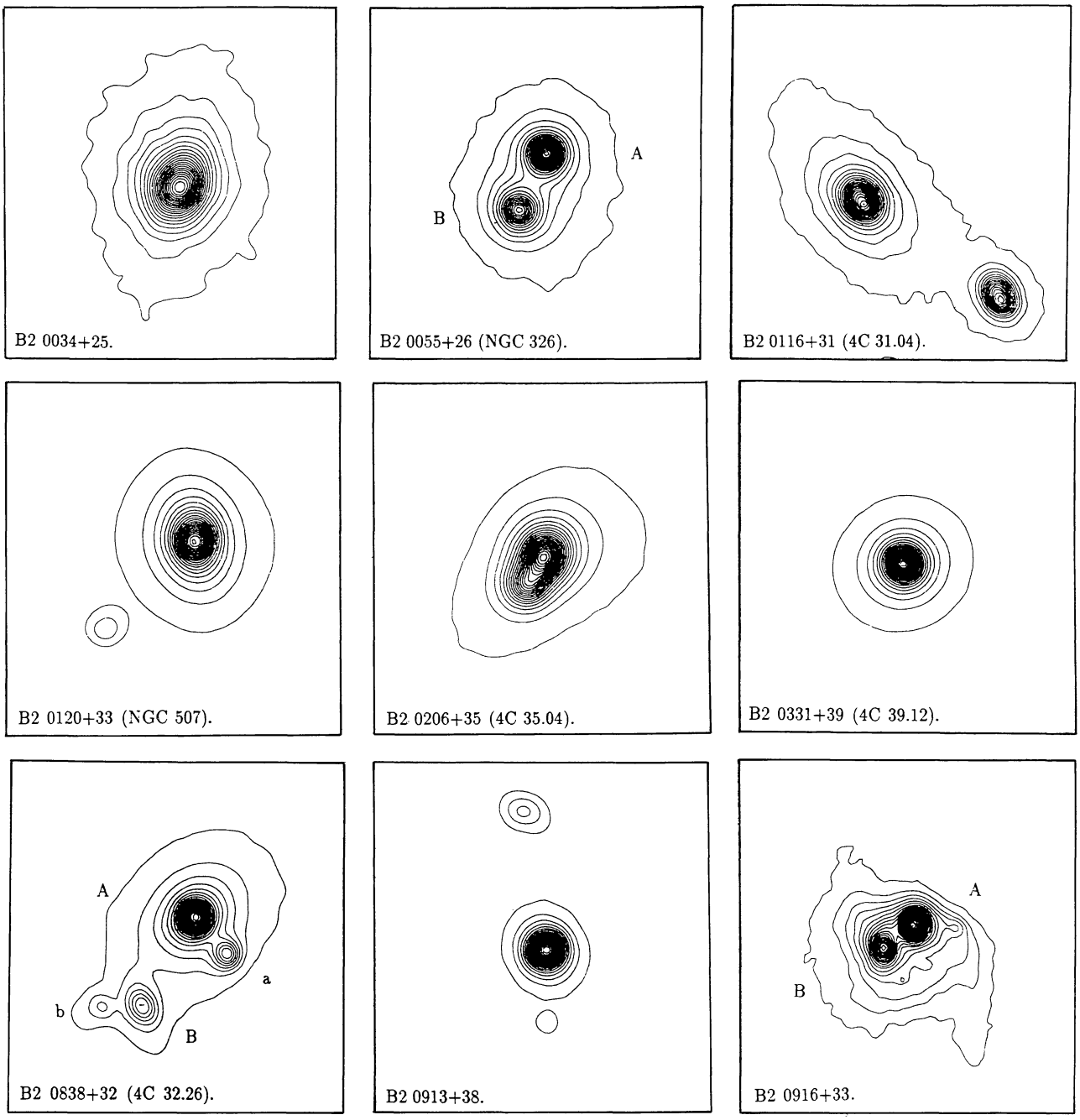

Fig. 2*a* Contour plots of *I*-band images of B2 radio galaxies from our sample. The convention used for these multiple component systems is a follows: galaxies with companions are indicated by capital letters, A is the brighter and the rest are labelled in decreasing intensity; galaxies with hot spots, i.e., small components of low surface brightness, are labelled with lower case letters (a, b, ...) in order of decreasing brightness.

galaxy and companion in common environment, D = dust lane, T = tails, F = fans, S = shells. The tails (T) refer to narrow structures (3:1 ratio of length to width), they are not necessarily radial and could be curved. In some galaxies two tails are found (2T). The fans (F) are similar to the tails but they are wide (ratio $1 < 3$). The bridges (B) refer to structures that join a radio galaxy with an apparent companion. The shells (S) are filamentary curved structures. Dust lane structures (D) due to obscuration by dust are

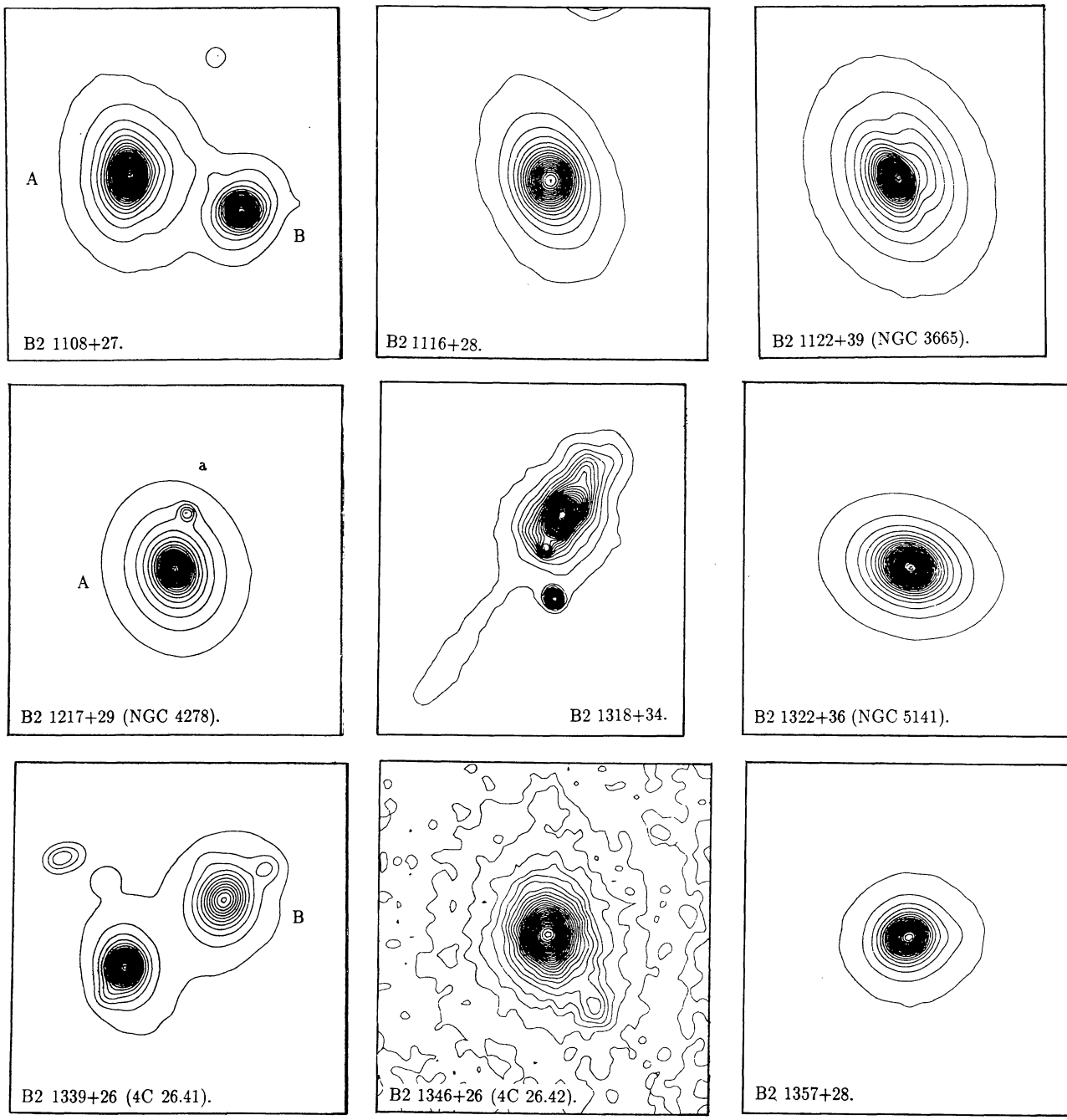

Fig. 2*b*. Same as Figure 2*a*.

clearly observed, some show a complex morphology. Few galaxies show boxy-shaped isophotes (BI) which are characteristic of merges. The presence of these peculiarities occur at different surface brightness levels (cf., contour maps) in the broad-band continuum images.

The morphological properties of the WRGs studied in this paper and presented in Table 4 can be summarized as follows:

1. *Normal galaxies* (37% of the sample). The WRGs that show elliptical symmetry are: 0034+25, 0331+39, 1116+28, 1322+36, 1357+28, 1422+26,

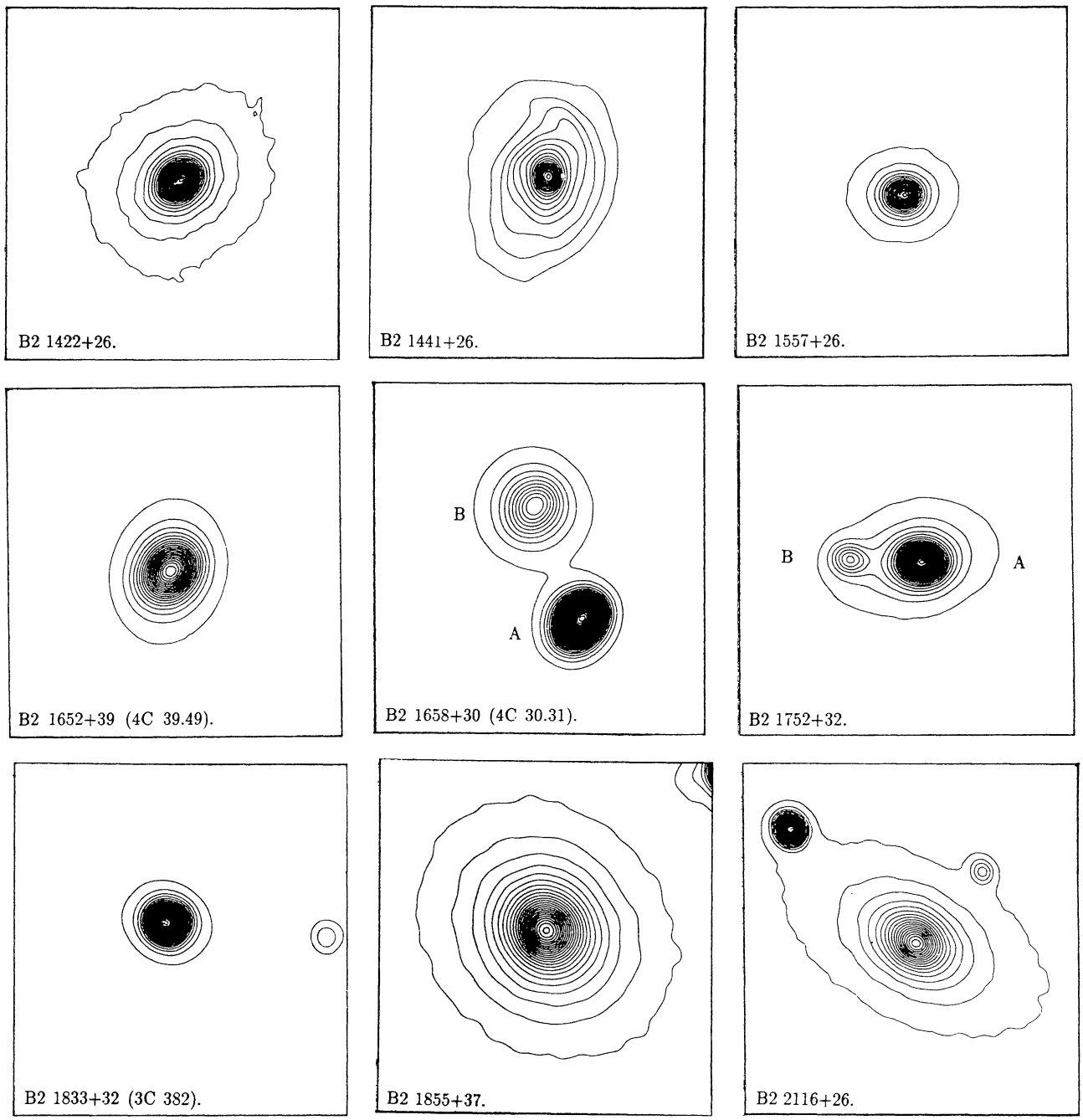

Fig. 2*c*. Same as Figure 2*a*.

1557+26, 1652+39, 1833+32, 1855+37; while 1441+26 shows a normal disk structure.

2. *Galaxies with companions* (73% of the sample). This means that most WRGs are located in a rich galaxy density environment. The WRGs sample shows that several have one or more nearby companions: 0034+25, 0055+26, 0116+31, 0120+33, 0206+35, 0838+32, 0913+38, 0916+33, 1108+27, 1116+28, 1217+29, 1318+34, 1339+26, 1357+28, 1441+26, 1658+30, 1752+32, 1833+32, 1855+37, 2116+26, 2236+35, 2335+26. The presence of such companions might be the cause of galaxy activity

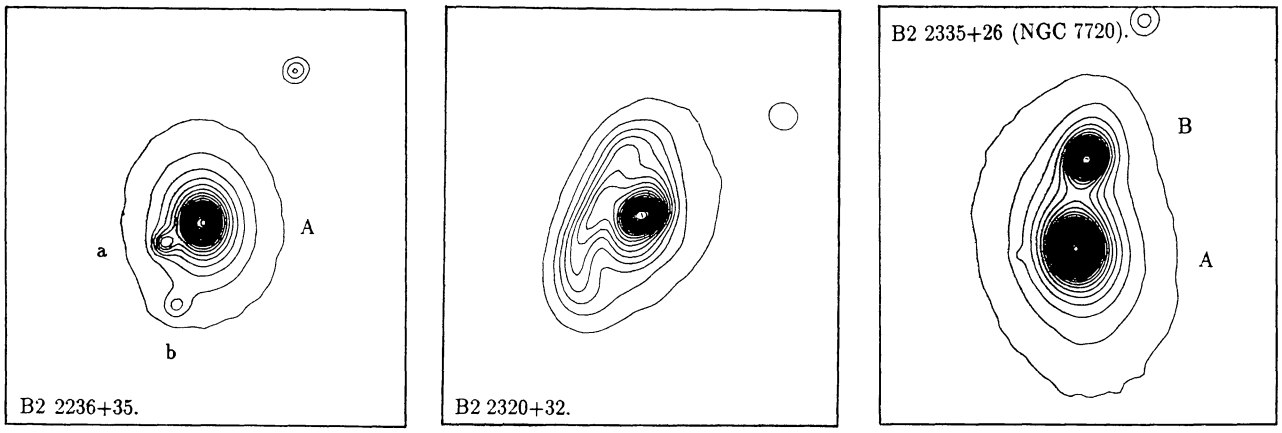

Fig. 2*d*. Same as Figure 2*a*.

and peculiarity. Furthermore, several galaxies with companions (50% of the whole sample), show the presence of a common surrounding and extended halo. These common halos are characteristic of E+E galaxy collisions or merges.

3. *Dust lanes* (7% of the sample). They are observed in two galaxies in our sample: 0206+35 (also reported by González-Serrano & Carballo 1993) and 1122+39 (Kotangi 1979). An important results is that in all cases, the radio structure lies perpendicular to the dust lane and that strong distortions of the surface brightness profiles are observed.

4. *Bridges, fans and tails.* Bridges (30% of the sample) between a main galaxy and its companion(s) are found in: 0055+26, 0838+32, 0916+33, 1108+27, 1339+26, 1658+30, 1752+32, 2236+35, and 2335+26. Fan-like structures (in 13%) are observed in: 0116+31, 0913+38, 1339+26, 2236+35. While tails (in 7%) were found in: 1346+26 and 2320+32.

5. *Boxy isophotes* (17%). Boxy-shapes isophotes are observed in: 0116+31, 1116+28, 1318+34, 2116+26, 2320+32. Most cases show an elliptical shape interior surrounded by a boxy external structure.

The morphological peculiarities are produced by galaxy interaction or merging of E+E, S+S or mixed pairs (e.g., Toomre & Toomre 1972; Toomre 1977; Quinn 1984). The theoretical simulations of galaxy interactions show that to produce tails a disk galaxy is required, the shells (Quinn 1989; Quinn & Hernquist 1987), are produced by the capture of a small S or E galaxy by a giant elliptical, the fans are produced by two giant ellipticals and dust lanes are the by-product of two E galaxies encounter (Merritt & Zeeuw 1983). The presence of extended haloes are similar to those shown in E-E galaxy n-body interaction models where merging takes place (e.g., Aceves, Cruz-González, & Carrillo 1997). The extended haloes are produced by different dynamical effects on the core and halo of the merging galaxies, the halo responds slower to the collision effects and distortions from the core geometry are produced in the external part of the galaxies.

5.2. Position Angles

In Table 7 we summarize the results from the VLA observations of the WRGs. The data was obtained from the following papers: Parma et al. (1986); de Ruiter et al. (1986); Fanti et al. (1986); Fanti et al. (1987); Parma et al. (1987); Morganti et al. (1987); Capetti et al. (1993). The contents of this table are: col. 1, source; col. 2, size of the radio emitting region (jet, lobe, halo, tail, wing) in arcsec; col. 3, position angle of the radio region; col. 4, the difference in optical and radio position angles (ΔPA).

No relation is obtained from the comparison of the optical and radio position angles of the WRGs. Radio galaxies of high redshift ($z \sim 1$) have their radio axis aligned with the semimajor axis of the optical continuum (e.g., Chambers, Miley, & van Breugel 1987; Mc Carthy et al. 1988), but radio galaxies of moderate redshift (Baum & Heckman 1989a) do not show any correlation. The WRGs studied here are consistent with the latter.

5.4. Environment in B2 Galaxies

As has been discussed above, several galaxies show nearby companions and in some cases the images show one or more maxima associated with the radio source position. It seems then, that most WRGs are located in a rich environment of galaxy density. Furthermore, several galaxies are in a known cluster or group of galaxies (30% of the sam-

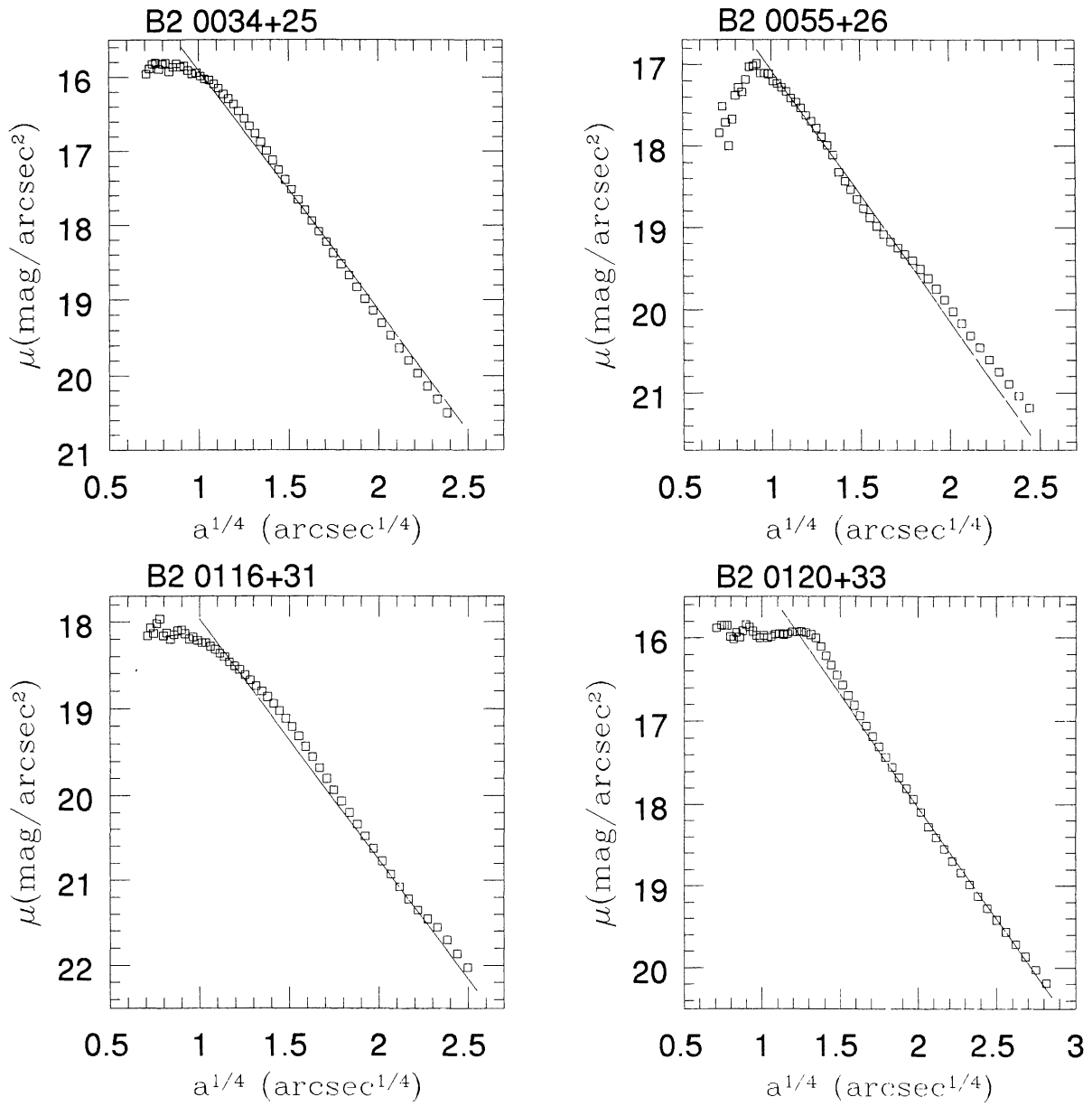

Fig. 3*a*. Observed surface brightness in the I-band versus the fourth root of the major axis, for B2 radio galaxies from our sample. The solid lines represent the de Vaucouleurs law.

ple): 0055+26 (group), 0116+31 (group), 0120+33 (Zwicky 0107+3212, Piscis group), 0838+32 (Abell 695), 1339+26 (Abell 1775), 1346+26 (Abell 1795), 1855+37 (group), 2236+35 (group) and 2335+26 (Abell 2634).

Of the 9 galaxies in cluster or group, only in three X-ray emitting haloes have been reported: 1339+26 (Abell 1775), 1346+26 (Abell 1795) and 2335+26 (Abell 2634) (Jones et al. 1979). The presence of these haloes is important because one possibility for the existence of emission-line regions is that they can produced by cooling accretion flows of the X-ray gas onto the dominant galaxy (Heckman 1981). In this picture the X-ray gas in the cores of the galaxy cluster can cool by thermal instabilities and accrete onto the slow moving dominant galaxy.

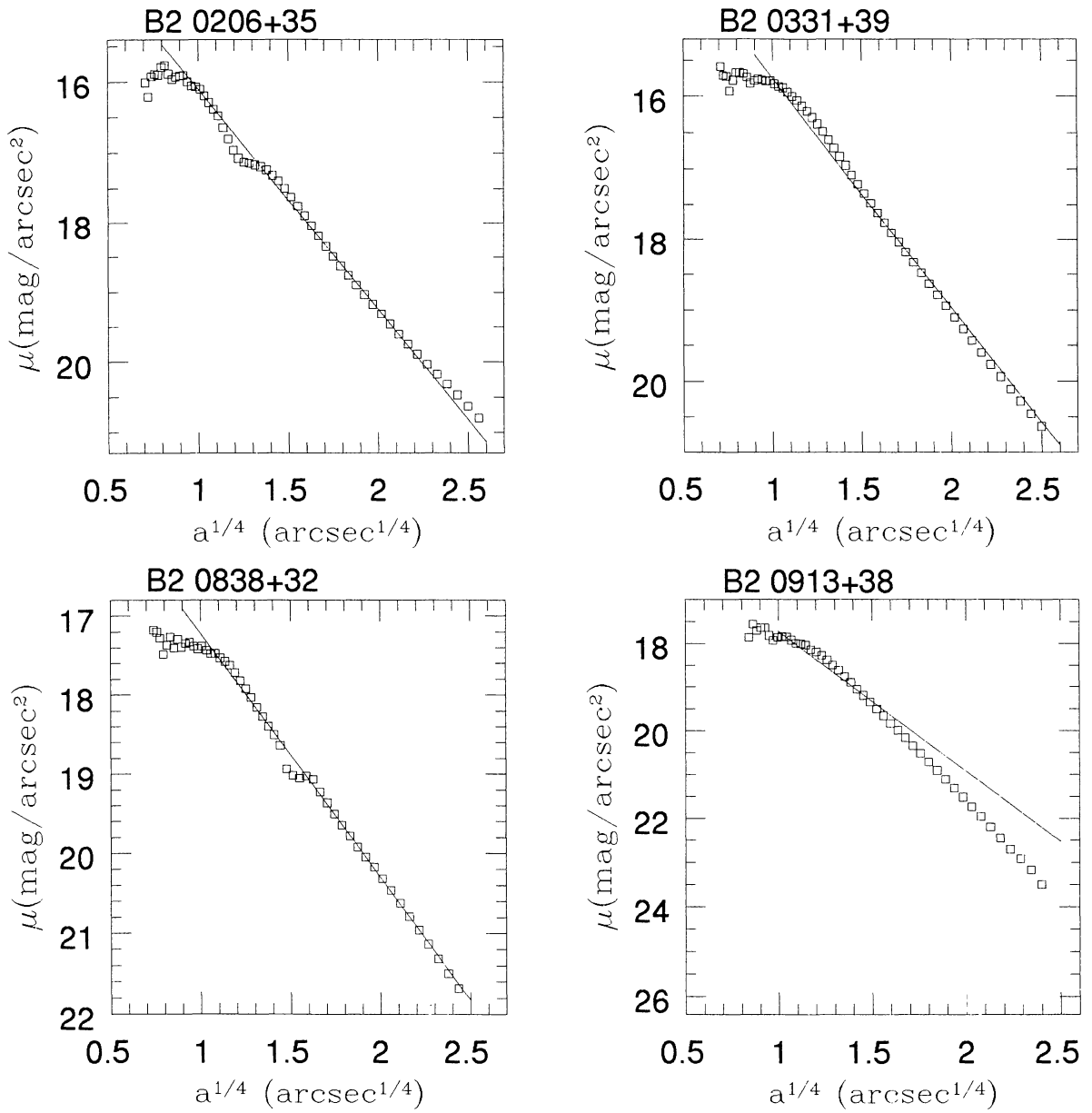

Fig. 3*b*. Same as Figure 3*a*.

5.4. Colors

Since galaxy interactions could trigger starburst activity, we decided to study the galaxy colors $(V - R)$ and $(R - I)$ derived from the aperture photometry, for clues on this problem. In Figure 4 we present a color-color diagram of the WRGs alone, while in Figure 5 we present the WRGs together with normal elliptical galaxies (Poulin 1988), quasars and BL Lac objects (Moles et al. 1985), and Seyfert galaxies (Hamuy & Maza 1987). As can be seen most WRGs concentrate in a region of this diagram, in the region dominated by AGNs and below the region of normal ellipticals and the bulges of spirals. Normal ellipticals are redder in $(R-I)$ than most AGNs and WRGs. The locus of WRGs is indicative of star formation activity, AGN activity or both.

There are seven WRGs that stand-out in this diagram. Three are extremely blue in $(V - R)$ and extremely red in $(R - I)$: 0916+33, 1116+28 and 1752+32, and are located in a region where no E galaxies or AGNs are found. $(V - R)$ of WRGs is similar to AGN values but three sources are redder: 1339+26, 1346+26 and 1658+30 (reddest), also in

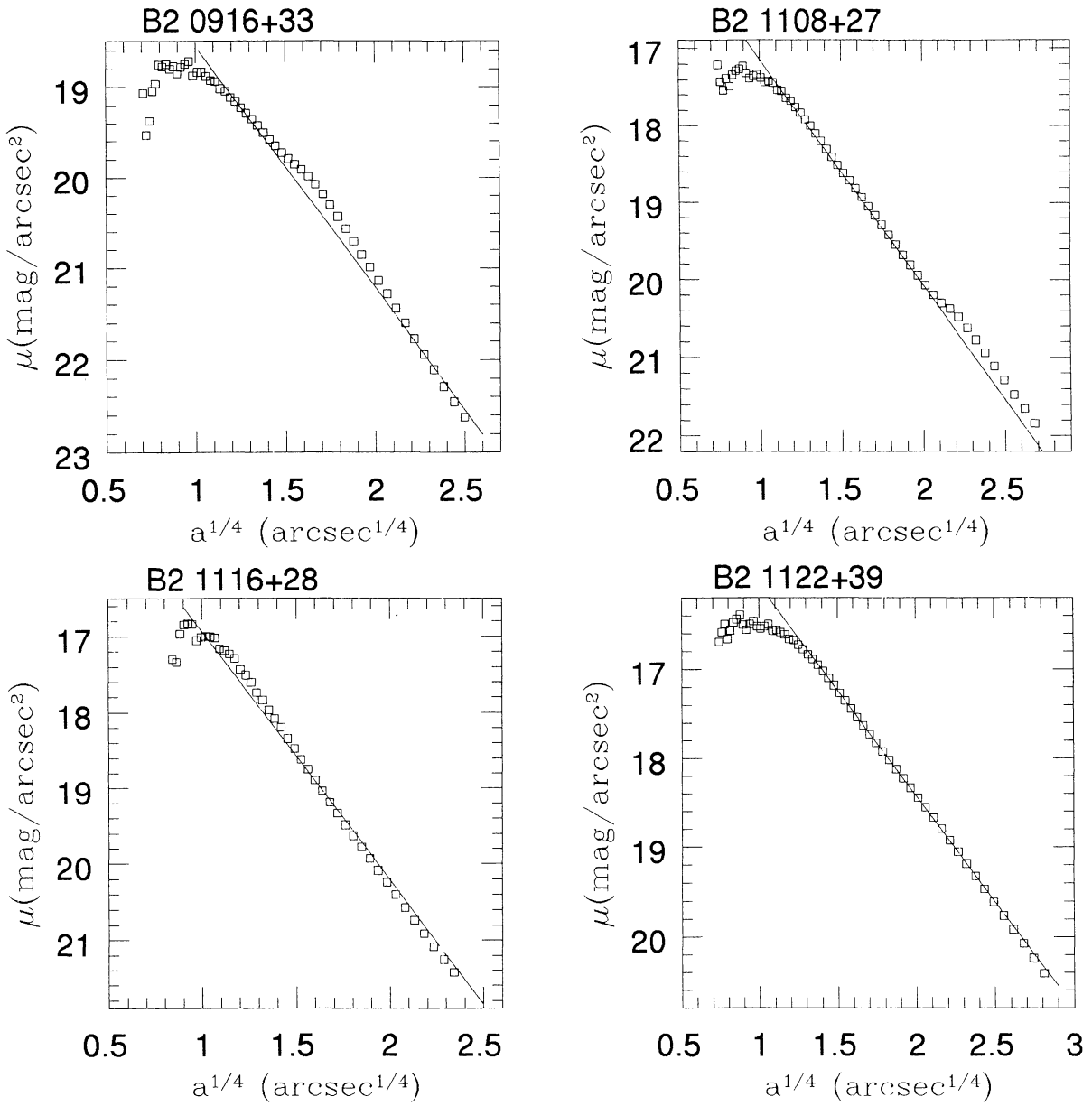

Fig. 3*c*. Same as Figure 3*a*.

a peculiar region of this diagram. The remaining source 1122+39 is blue in $(R-I)$ in a region associated with some BL Lac objects and quasars.

An inspection of the photometry presented in Table 4, of the optical morphology presented in Table 6 and of the individual galaxy description presented in § 5.6, allows us to conclude that most galaxies with unusual colors have peculiar morphology and/or galaxy companions. The extremely blue galaxies 0916+33 and 1752+32 have bridges in their structure, while 1116+28 has boxy isophotes which are all evidence of galaxy interaction; of the extremely red WRGs 1658+30 is a pair of E galaxies with a bridge, while 1339+26 and 1346+26 are in a galaxy cluster.

For very powerful radio galaxies (FRII) with peculiar optical morphologies, this effect is also found by Heckman et al. 1986: the $(B-V)$ colors are bluer than normal ellipticals. But no work has been reported for colors as $(V-R)$ or $(R-I)$. We conclude that all radio galaxies with peculiar optical morphologies are significantly more likely to have recent, or on-going, star formation. The role of possible starburst activity can only be answered with imag-

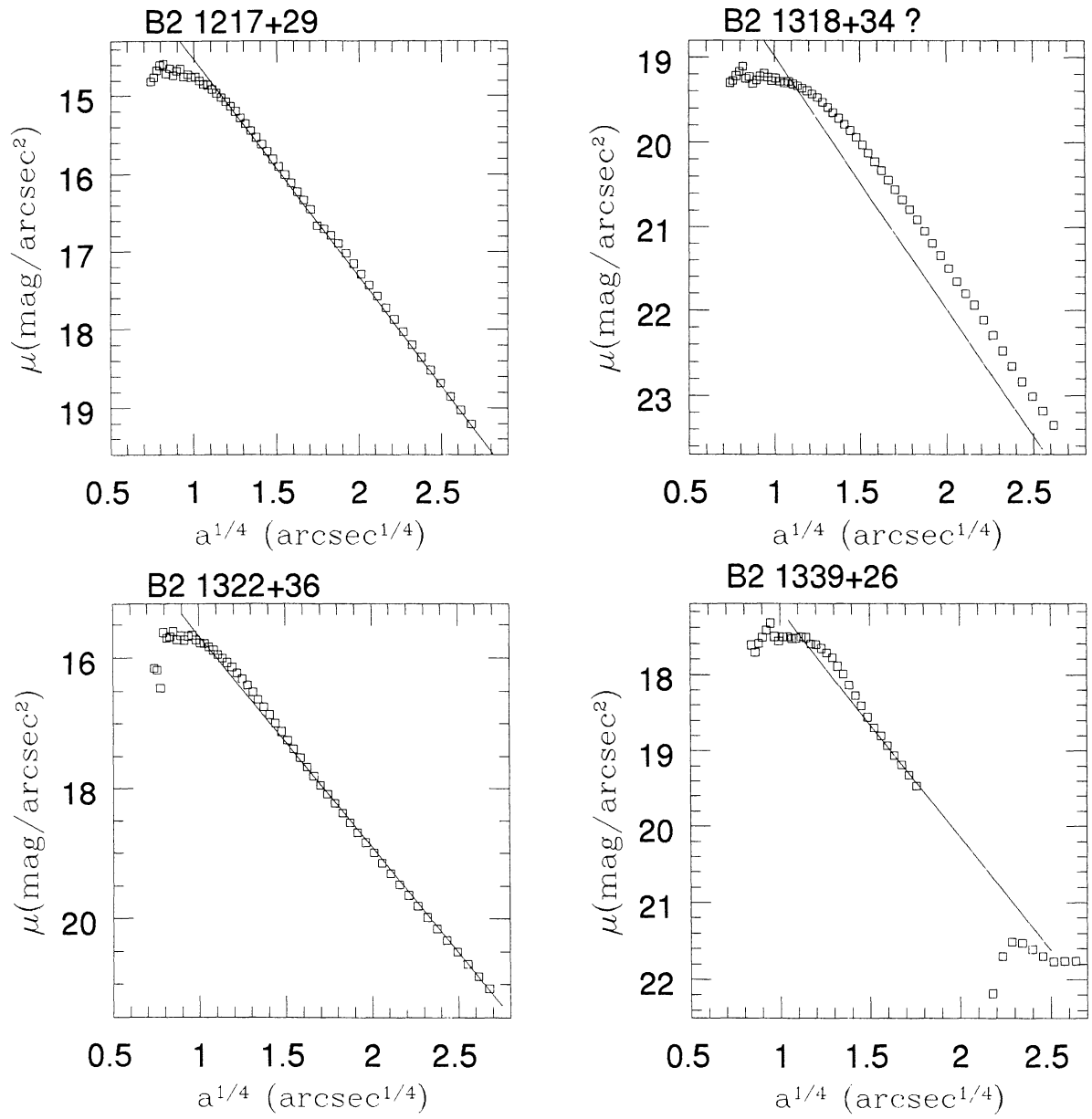

Fig. 3*d*. Same as Figure 3*a*.

ing studies in the near infrared (Cruz-González et al. 1997).

5.5. Surface Brightness Profiles

We divided the surface brightness profiles of elliptical galaxies in our sample into three groups, according to the degree of possible tidal influence by their neighbors, following Kormendy (1977) classification. The WRGs in our sample can be grouped in three classes:

1. Class T1. There are no neighbors of any importance, so the objects should be dynamically isolated (47% of the WRGs): 0034+25, 0206+35 (peculiar), 0331+39, 1116+28, 1122+39, 1217+29, 1322+36, 1346+26, 1422+26, 1557+26, 1855+37, 2116+26.
2. Class T2. An intermediate group is required where the degree of tidal influence is unclear. It includes luminous galaxies with fainter companions (13%): 0120+33, 0838+32, 1357+28, 1652+39 (peculiar), 1833+32 (peculiar), 2236+35.

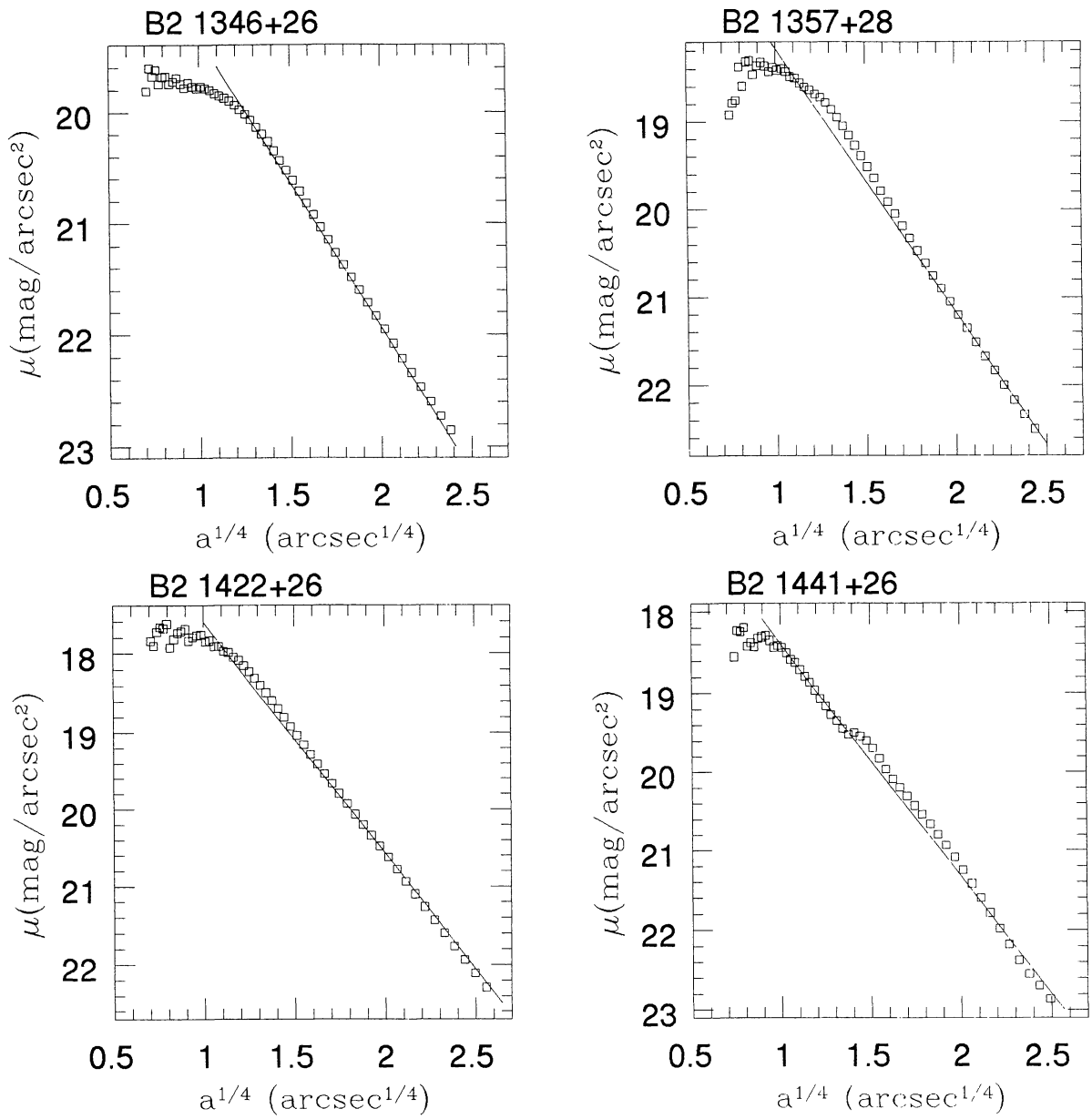

Fig. 3*e*. Same as Figure 3*a*.

3. Class T3. These are galaxies which have at least one companion of comparable or greater brightness located within several diameters (23%): 0055+26, 0116+31, 1108+27, 1339+26, 1658+30, 1752+32, 2335+26.

An examination of the surface brightness profiles (cf., Figs. 3*a* to 3*h*), shows that galaxies with non de Vaucouleurs law profiles are all of classes T2 or T3. However, in some cases some portions of the profile do follow a de Vaucouleurs law. We conclude that tidal effects modify the external portions of the WRGs light profiles. The group T1 successfully reproduces the light curve of a galaxy with a de Vaucouleurs $r^{-1/4}$ law, but in all cases the profiles show a turnover, small bump, or flatness, in the innermost regions, which could correspond to an additional light component in the profile (nuclear excess). This peculiarity in the internal parts of the radial profiles is also observed in class T2 and T3 galaxies. We conclude that most WRGs (83%) show the inter-

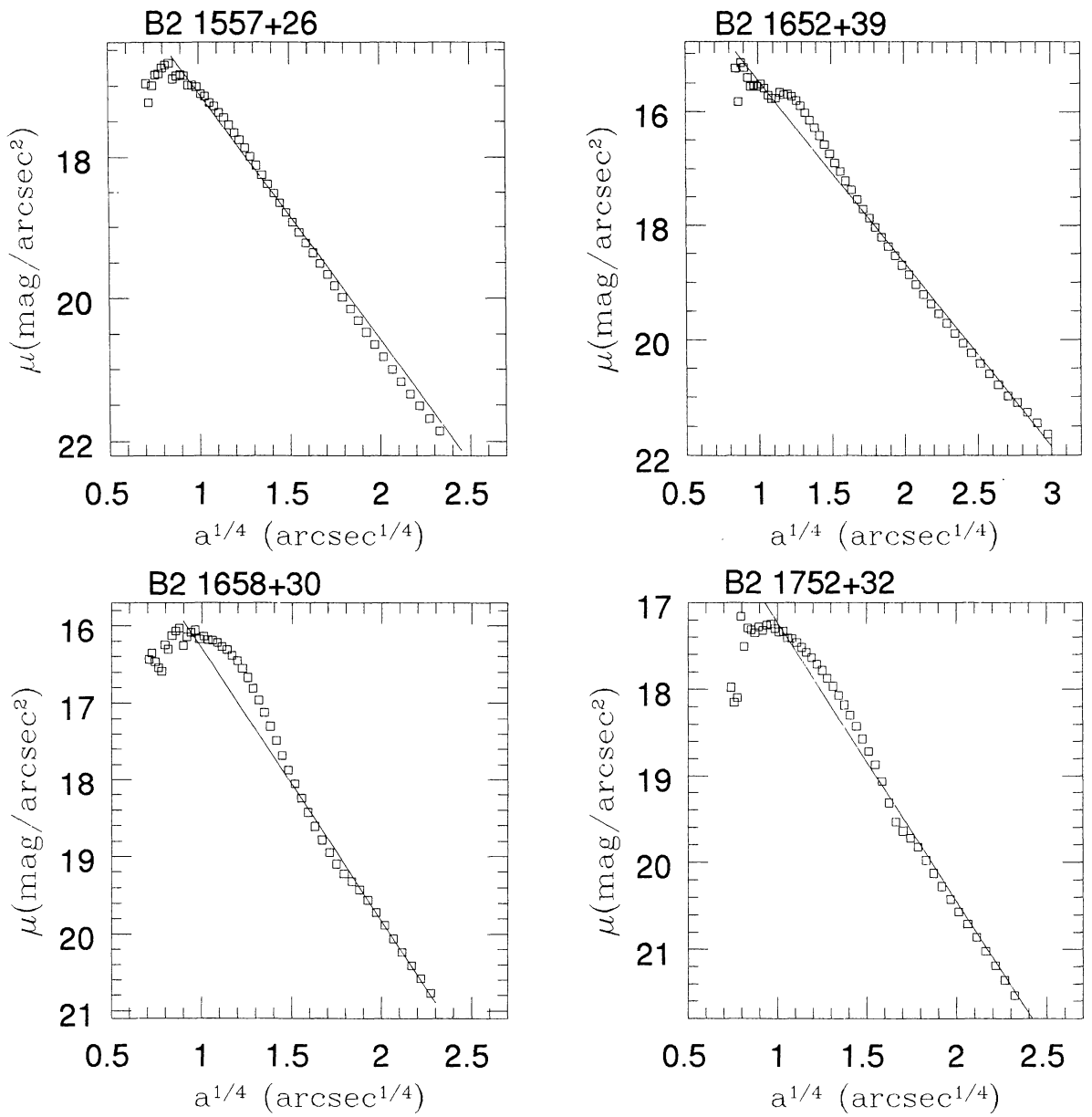

Fig. 3*f*. Same as Figure 3*a*.

nal turnover or deviation from de Vaucouleurs type profiles produced by a nuclear emission source.

There are few WRGs with rather peculiar profiles: 0206+35 has a kink that can be explained by a dust lane; while 1652+39 (which is classified as a BL Lac) and 1833+32 (broad line radio galaxy) deviate from the $r^{-1/4}$ law either internally or externally, and should be in class T2 contrary to their morphology which classifies both as T1. Although we find no evidence in these two WRGs for tidal influence their profiles clearly indicate that they are in interaction and/or that the nuclear activity modifies the overall profile.

For spiral galaxies the surface brightness profiles do not follow the $r^{-1/4}$ law as expected, i.e., 0916+33, 1441+26 and 2320+32.

Two extreme cases were detected. First, the peculiar galaxy 1318+34 where the profile follows a curve with a slope of $-1/4$ but the observed curve is above the de Vaucouleurs law. Second, the elliptical

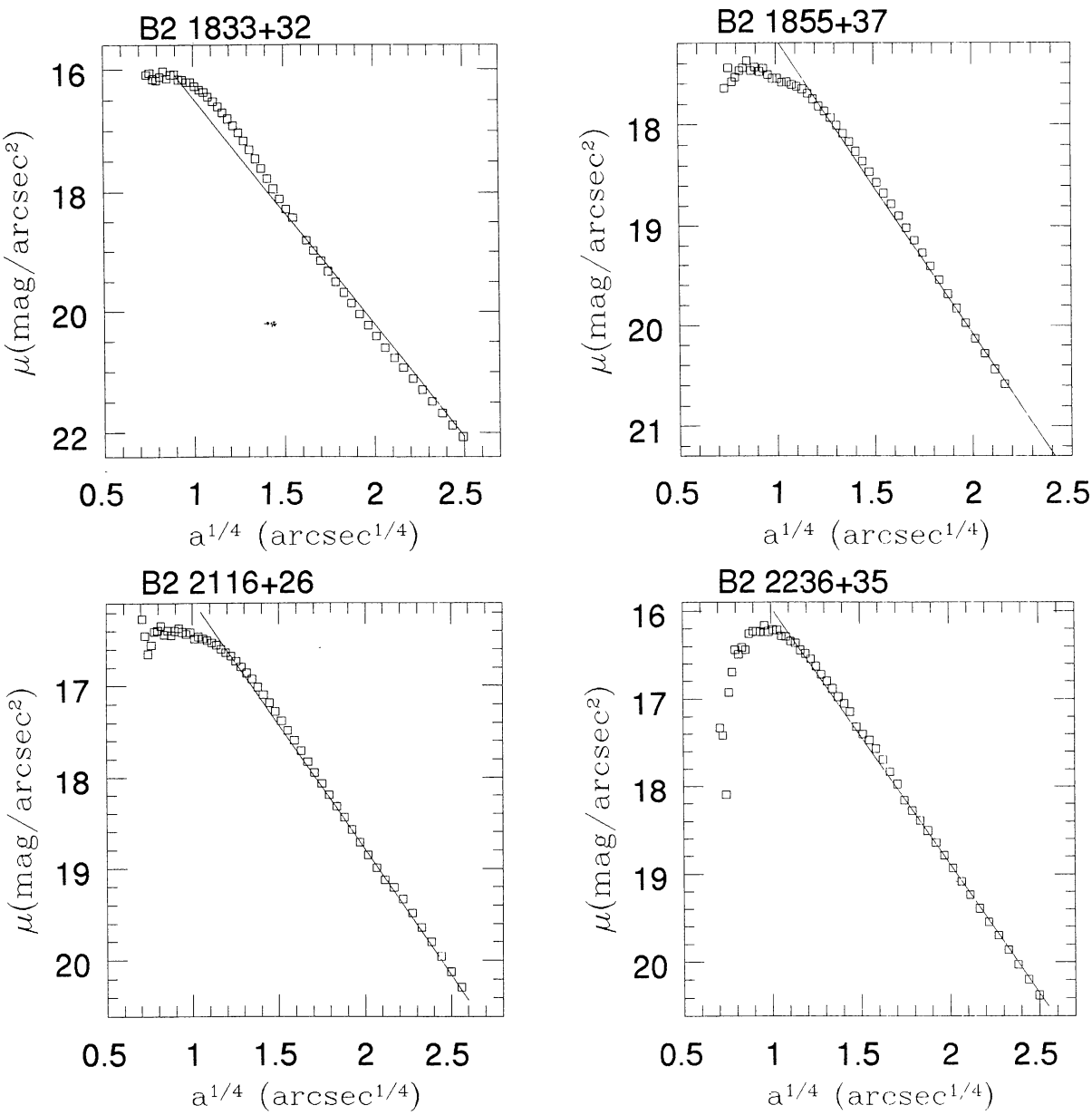

Fig. 3*g*. Same as Figure 3*a*.

galaxy 0913+38 whose profile is much steeper than an $r^{-1/4}$ law and very complex. From its morphology we would expect a class T2 or T3 profile, but this is not the case.

The tidal effects evident in outer parts of the WRGs profiles, are consistent with Kormendy's conclusion that elliptical galaxies with nearby companions of comparable luminosity have bright envelopes above the extrapolation of a de Vaucouleurs law fitted to the inner parts, and that these envelopes are greatly reduced or absent in isolated galaxies. Furthermore, most WRGs show evidence of an additional nuclear component which introduces a turnover in the innermost portions of the profiles as compared to normal ellipticals.

6. INDIVIDUAL GALAXY RESULTS

A brief description of the individual galaxies studied in this paper is presented in this section, which

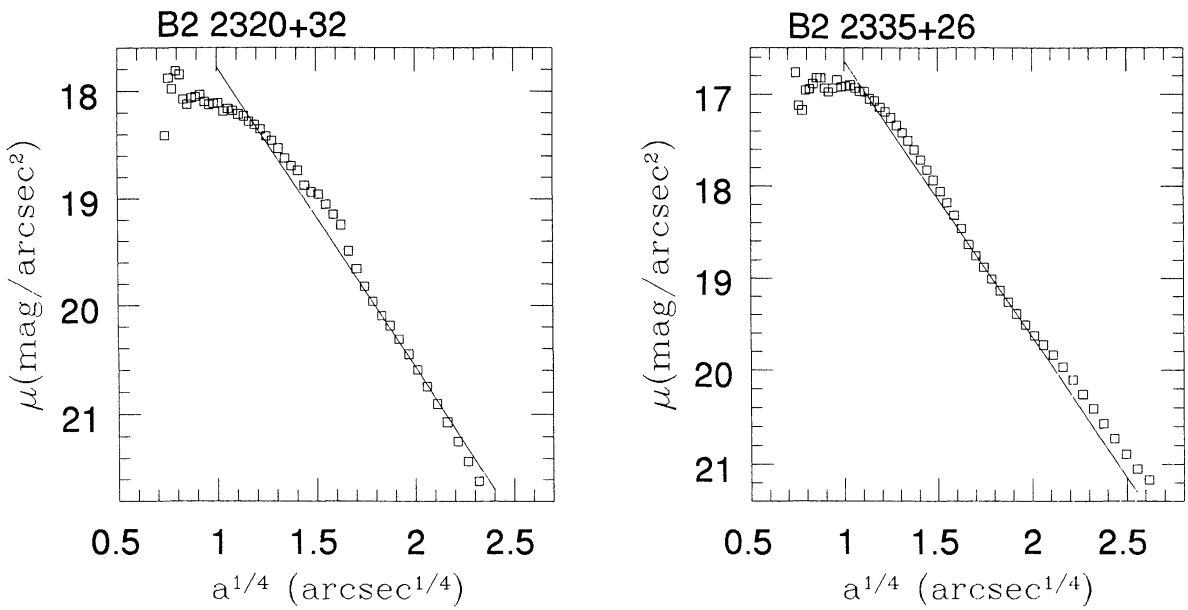

Fig. 3.*h*. Same as Figure 3*a*.

TABLE 6

MORPHOLOGICAL PROPERTIES

Source B2 (1)	Components[a] (2)	Source B2 (1)	Components[a] (2)
0034+25	NE	1339+26	CE, B, F
0055+26	CE, B	1346+26	T
0116+31	CE, F, BI	1357+28	NE
0120+33	CE	1422+26	NE
0206+35	D	1441+26	ND
0331+39	NE	1557+26	NE
0838+32	CE, B	1652+39	NE
0913+38	CE, F	1658+30	CE, B
0916+33	CE, B	1752+32	CE, B
1108+27	CE, B	1833+32	NE
1116+28	NE, BI	1855+37	NE
1122+39	D	2116+26	CE, BI
1217+29	CE	2236+35	CE, B, F, BI
1318+34	2T, CE, BI	2320+32	S, 2T
1322+36	NE	2335+26	CE, B

[a] NE = normal E galaxies, ND = normal disk galaxies, B = bridge between galaxy and companion, CE = radio galaxy and companion in common environment, D = dust line, T = tails, F = fans, S = shells, BI = boxy-shaped isophotes.

TABLE 7

RADIO PROPERTIES

Source	Size[a]	PA	Source	Size[a]	PA
B2	(″)	(°)	B2	(″)	(°)
(1)	(2)	(3)	(1)	(2)	(3)
0034+25	40 E_{jet}	90	1346+26	10 ext.	21
	40 W_{jet}	...	1357+28	28 N_{jet}	180
0055+26	2.3 $EW_{ext.}$	94		26 S_{jet}	...
0116+31	core	...	1422+26	24 E_{jet}	$\sim$ 93
0120+33	60 $E_{lob.}$	$\sim$ 98		27 W_{jet}	...
	60 $W_{lob.}$	...		50 $E_{lob.}$	...
0206+35	34 SE_{jet}	$\sim$124		60 $W_{lob.}$	...
	33 NW_{jet}	...	1441+26	120 $E_{lob.}$	$\sim$ 70
0331+39	68 halo	165		80 $W_{lob.}$	...
0838+32	110 W_{tail}	~ -80	1557+26	2.3 A	$\sim$ 64
	15 NE_{wing}	$\sim$ 25		0.8 B	$\sim$102
0913+38	$>$ 8 E	$\sim$ 90	1652+39	core	97
	17 W	...	1658+30	48 SW_{jet}	~ -125
0916+33	core	...		80 $NE_{lob.}$	$\sim$ 65
1108+27	25 E_{jet}	$\sim$ 80		70 $SE_{lob.}$	...
	40 W_{jet}	...	1752+32	$\sim$25 NE_{jet}	$\sim$ 55
1116+28	50 E_{jet}	$\sim$ 80		$\sim$40 SW_{jet}	...
	75 W_{jet}	~ -65	1833+32	90 $NE_{lob.}$	$\sim$ 59
1122+39	34 SE_{jet}	$\sim$130		$\sim$50 $SW_{lob.}$	...
	40 NW_{jet}	...	1855+37	6 $N_{lob.}$	15
1217+29	$\sim$0.03 halo	~ -60		2 $S_{lob.}$	44
1318+34	core	146	2116+26	40 N_{jet}	22
1322+36	27 S_{jet}	$\sim$ 0		40 S_{jet}	...
	22 $N_{lob.}$	...	2236+35	24 NE_{jet}	44
	25 $S_{lob.}$	...		22 SW_{jet}	...
1339+26	198 HT[b]	$\sim$ 25	2335+26	360 NS_{tail}	180
	24 WAT[c]	...		324 EW_{tail}	...

[a] Size and type of radio structure.
[b] Head tail radio galaxy.
[c] Wide angle tail radio galaxy.

includes the morphology and surface brightness profile results.

B2 0034+25. Galaxy in the Zwicky cluster 0034.4+2532, a companion is located at $\sim 44''$ to the SE, and the radio galaxy is the 3^{rd} brightest cluster member. The images presented here (cf., Fig. 1*a*) correspond to the optical counterpart of the radio galaxy. At V, R, and I the images show normal E galaxy contours (NE, Fig. 2*a*) and our fits indicate an $r^{-1/4}$ intensity profile (Fig. 3*a*, T1). There is not a strong indication of interaction with the SE companion, as discussed by González-Serrano & Pérez-Fournon (1991), nor clear indications of other strong peculiarities.

B2 0055+26 (NGC 326). Galaxy pair in a common halo (cf., Fig. 1*a*). The contour map in Fig. 2*a* shows the common halo and the two E-like components. The most luminous source located to the NW is associated with the radio emission. The intensity profile shown corresponds to both nuclear components (Fig. 3*a*) and is class T3. A third galaxy is located to the SW and some traces of possible interaction (bridge and contour distortions) could be seen in the R frame.

B2 0116+31 (4C 31.04). Galaxy pair in a common halo (cf., Fig. 1*a*). The contour map in Fig. 2*a* shows elliptical like contours in the internal part and a common halo which distorts them in the external part. The most luminous source located to the NE is associated with the radio emission. The intensity profile shows both components (Fig. 3*a*, T3).

B2 0120+33 (NGC 507). Galaxy in the Zwicky

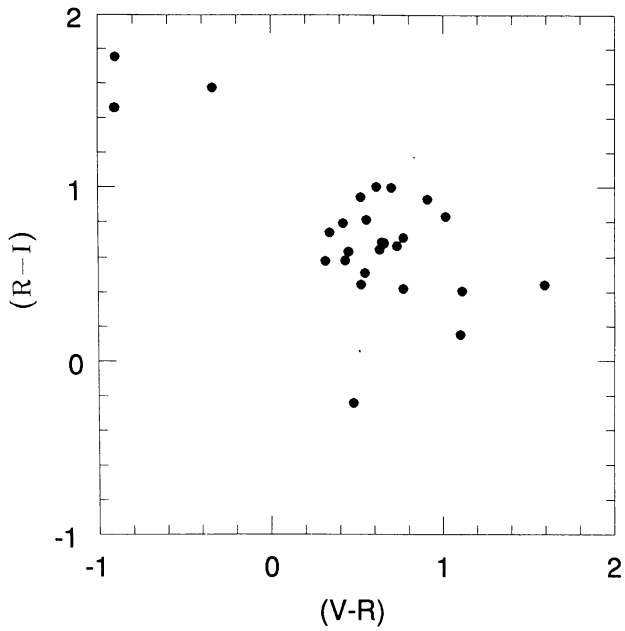

Fig. 4. Plot of $(V - R)$ versus $(R - I)$, for the radio sources from our sample.

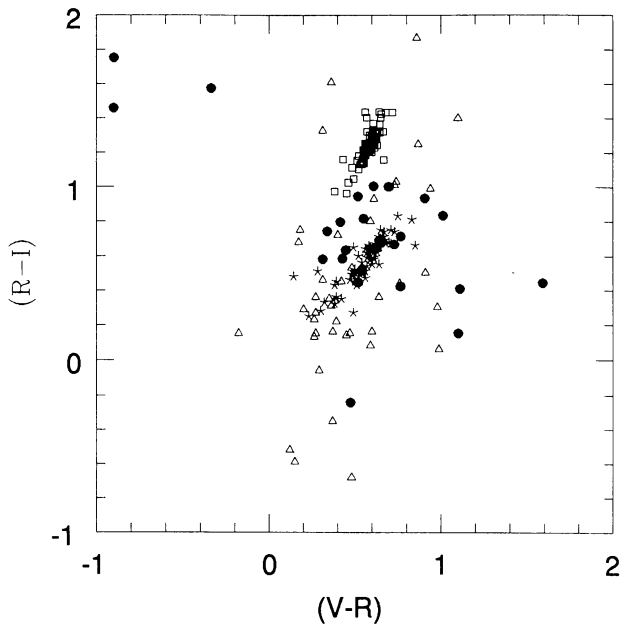

Fig. 5. Plot of $(V - R)$ versus $(R - I)$, for the radio galaxies from our sample, [filled circles], compared with: quasars and BL Lac objects (Moles et al. 1985), [triangles]; Seyfert galaxies (Hamuy & Maza 1987), [stars]; and normal E galaxies (Poulin 1988), [squares].

cluster 0107+3212, it is either the brightest or second member in the cluster. In its halo a weak component is detected to the SE of the nucleus (cf., Fig. 1*a*). The contour map in Fig. 2*a* shows an elliptical shape and the intensity profile does not follow an $r^{-1/4}$ law (Fig. 3*a*) since a kink is present in the external part (T2).

B2 0206+35 (4C 35.04). Galaxy with a dust lane that extends from NE to SW (cf., Fig. 1*a*). Three fainter components to the SW are clearly detected. The radio extended emission is perpendicular to the dust lane. The non-elliptical isophotes and the companions are indicative of a tidal interaction (Fig. 2*a*). CCD surface photometry also obtained by González & Pérez-Fournon (1991). Since the dust lane is almost perpendicular to the major axis, the intensity profile shows clearly a distortion from the $r^{-1/4}$ law at the dust lane location (Fig. 3*b*, T1 peculiar).

B2 0331+39 (4C 39.12). Normal elliptical galaxy with no traces of interaction (cf., Fig. 1*a*), the halo contours follow the internal ones (Fig. 2*a*) and the intensity profile follows the $r^{-1/4}$ law (Fig. 3*b*, T1).

B2 0838+32 (4C 32.26). In the literature this source appears as a double system in a common halo where the brighter galaxy is the center of Abell 695 cluster. We found a multiple system with at least four galaxies in a common halo (cf., Fig. 1*a*), also clearly shown in the contour map of Fig. 2*a*. The brighter galaxy component is associated with the SE component. The intensity profile shows a distortion from the $r^{-1/4}$ law at the other components location (Fig. 3*b*, T2).

B2 0913+38. Galaxy with two companions at distances $< 45''$ one to the N and one to the S. The image shows an E galaxy with the external contours slightly distorted, probably due to a weak interaction with the companions (Figs. 1*a* and 2*a*). The intensity profile is steeper than an $r^{-1/4}$ law (Fig. 3*b*).

B2 0916+33. The structure in this galaxy resembles a spiral galaxy with a double nucleus (Fig. 1*a*). It is a system similar to late type systems found in *IRAS* Markarian galaxies (e.g., Mazzarela & Boroson 1993). The nucleus to the NW is the brightest and in one arm a possible H II region is resolved (image at R, and Fig. 2*a*). The intensity profile for this galaxy is distorted (Fig. 3*c*).

B2 1108+27. This is a pair of elliptical galaxies with traces of interaction, here the eastern component corresponds to the radio emission (Fig. 1*b*). The contour map of this E+E pair in Fig. 2*b*, shows a common halo and external contour distortions. The $r^{-1/4}$ profile shows a kink at large radii (Fig. 3*c*, T3).

B2 1116+28. The images show an elliptical galaxy with no traces of interaction (Fig. 1*b*). A companion to the east is detected which is spatially

related to the very extended radio emission. The contour map shown in Fig. 2*b* shows an E-type structure and the intensity profile follows an $r^{-1/4}$ (Fig. 3*c*, T1).

B2 1122+39 (NGC 3665). This elliptical galaxy has a dust lane (e.g., Kotanyi 1979). The images show this dust lane with direction NE to SW (Fig. 1*b*). As in other cases (e.g., Kotanyi & Ekers 1979) the radio emission is almost perpendicular to the dust lane. The dust lane is almost parallel to the major axis (Fig. 2*b*) and the intensity profile follows an $r^{-1/4}$ law (Fig. 3*c*, T1).

B2 1217+29 (NGC 4278). Radio galaxy with a companion to the NW in the same halo (Fig. 1*b*). The contour map shows no distortion (Fig. 2*b*) and the profile follows an $r^{-1/4}$ (Fig. 3*d*, T1).

B2 1318+34? This is a very peculiar galaxy (Fig. 1*b*) with two almost perpendicular tails, to the SE and SW. In the central region there are at least 3 maxima and the contours are clearly distorted to almost boxy-like (Fig. 2*b*). The brightness profile shows a kink in the external part and has a slope of $-1/4$, but is below the de Vaucouleurs law (Fig. 3*d*). This galaxy identification as a B2 is uncertain (Fanti et al. 1987).

B2 1322+36 (NGC 5141). Our image (Fig. 1*b*) and contour map (Fig. 2*b*) show basically an elliptical galaxy, and the brightness profile follows an $r^{-1/4}$ law (Fig. 3*d*, T1). Signs of interaction with NE companion, NGC 5142, at 2.3′ (González-Serrano & Carballo 1993) which has boxy like isophotes, apparently affect the radio structure of NGC 5141 (slightly distorted jet morphology, e.g., Capetti et al. 1993) but not the stellar continuum.

B2 1339+26 (4C 26.41). Galaxy pair in the center of Abell 1775 cluster. The radio emission is associated with the SE galaxy which is more luminous. Our images (Fig. 1*b*) show five sources in the same halo. The NE emission coincident with the extended radio emission; Simon (1979) shows that the brighter source corresponds to a "head tail" radio galaxy while the NE is a "wide angle tail". Fig. 2*b* shows non-elliptical intensity contours possibly due to the interaction. The intensity profile show both galaxies (Fig. 3*d*, T3).

B2 1346+26 (4C 26.42). This is the brightest galaxy in the cluster Abell 1795. The image of this cD galaxy (Fig. 1*b*), shows an extension to the SW, also shown in the contour map in Fig. 2*b*. The intensity profile does not follow an $r^{-1/4}$ law (Fig. 3*e*, T2). This galaxy has been well studied by van Breugel, Heckman, & Miley 1984; it has extended emission-line nebulae spatially coincident with the radio continuum emission (see VLA map of O'Dea, Gallimore, & Baum 1995) and anti-correlated with the radio polarization; being a similar case to powerful radio galaxies as 3C 277.3 (Miley et al. 1981).

B2 1357+28. This galaxy shows no traces of strong peculiarities (Fig. 1*b*). Two nearby galaxies located to the W within 45″ may be producing a small distortion in the external contour (Fig. 2*b*). The intensity profile is class T2 (Fig. 3*e*).

B2 1422+26. This galaxy shows no traces of strong peculiarities (Fig. 1*c*) and is a normal elliptical both in morphology (Fig. 2*c*) and in an $r^{-1/4}$ profile (Fig. 3*e*, T1).

B2 1441+26. The image of this galaxy shows a nearly face-on spiral pattern with two companions to the E and NE of the nucleus at distances $< 30''$ (Fig. 1*c*). The contour map shows an inner structure typical of a stellar bulge or maybe a bar with a spiral pattern (Fig. 2*c*). The intensity profile does not follow the $r^{-1/4}$ law (Fig. 3*e*).

B2 1557+26. This galaxy shows no traces of strong peculiarities (Fig. 1*c*), and is a normal elliptical both in morphology (Fig. 2*c*) and profile (Fig. 3*f*, T1).

B2 1652+39 (4C 39.49, Mk 501). This source is a well known BL Lac object (e.g., Ulrich et al. 1975). The images show an extremely compact source with a surrounding nebulosity (Fig. 1*c* and Fig. 2*c*). The intensity profile is class T2 (Fig. 3*f*).

B2 1658+30 (4C 30.31). This is a pair of galaxies (Fig. 1*c*) in a common halo, possibly two ellipticals, in which the most luminous one is to the SW (Fig. 2*c*) and is associated with the radio source. The intensity profile includes both galaxies (Fig. 3*f*) and follows an $r^{-1/4}$ law only in the external part (T3).

B2 1752+32. This is another E+E pair of galaxies (Fig. 1*c*) in a common halo, in which the most luminous one is to the W (Fig. 2*c*) and is associated to the radio source. The intensity profile includes both galaxies (Fig. 3*f*, T3).

B2 1833+32 (3C 382). This radio galaxy has a rather complex radio structure (Black et al. 1992), and from its radio structure closer to an FRII type source rather than a weak radio galaxy (FRI). The image (Fig. 1*c*) shows that it is in a dense group of galaxies with 3 nearby faint companions (E, W, and SE) at distances $< 30''$. The elliptical shape contours (Fig. 2*c*) may indicate a weak interaction with the western companion and the intensity profile is class T2 (Fig. 3*g*).

B2 1855+37. This galaxy is the brighter source in a group of galaxies (Fig. 1*c*). The elliptical-shape contours (Fig. 2*c*) indicate an E galaxy and the intensity profile follows an $r^{-1/4}$ law (Fig. 3*g*, T1)

B2 2116+26 (NGC 7052). The image shows an elliptical galaxy with a box-like structure (Fig. 1*c*) in a rich stellar field. This galaxy is well studied by González-Serrano & Pérez-Fournon (1991) who classified it as a boxy elliptical with a central structure. Our contour plot is presented in Fig. 2*c* and shows a possible companion to the NW at a distance $< 15''$

indicating that this galaxy is not a normal E galaxy; this evidence is also supported by Gallagher (1986) who reports a small nuclear dust lane, which is not evident in our CCD images. Contrary to this result, the intensity profile is class T1 (Fig. 3*g*).

B2 2236+35. The image (Fig. 1*d*) shows a possible cD galaxy with a group of galaxies in a common halo. The contour plot (Fig. 2*d*) shows that at least 2 galaxies to the SE are in the cD halo but the images show that maybe the NW source is also in it. The intensity profile (Fig. 3*g*, T2) shows two kinks due to the companions. The radio structure (Morganti et al. 1987) shows a NE to SW double-sided jet that extends $\sim 20''$ on each side.

B2 2320+32. This is a galaxy classified as a spiral but our observations show that the morphology is more of a peculiar galaxy (Fig. 1*d*). To the eastern part of the nucleus we found two tails or a shell extended structure (Fig. 2*d*) and a weak companion to the NW. The intensity profile shows clearly the presence of the tails (Fig. 3*h*).

B2 2335+26 (NGC 7720). Galaxy pair in the cluster Abell 2634, morphologically classified as a D galaxy. The brighter source is the southern one shown in Fig. 1*d*. This is a good example of a galaxy with a bridge, both galaxies have a common extended halo (Fig. 2*d*). This is a well studied source in the radio that presents curved and pronounced radio jets. The intensity profile shows the presence of the companion (Fig. 3*h*, T3).

7. CONCLUSIONS

The main results of the V, R, and I imaging study of 30 weak radio galaxies (WRGs), which involved morphological properties, surface photometry, colors, surface brightness profiles and radio versus optical properties, can be summarized as follows:

1. The WRGs morphologies show that most objects ($\sim$ 87% of the sample), are elliptical galaxies of diverse surface brightness, i.e., WRGs include galaxies from cD galaxies to low surface brightness E's. Few WRGs are spirals ($\sim$ 10%) and the remaining ones are peculiar galaxies.

2. About 63% of the host galaxies of WRGs show peculiarities in their optical morphologies.

3. The morphological peculiarities are made evident by structures at larger and/or smaller scales such as fans, tails, shells, dust bands and double nuclei, which are somewhat similar to structures obtained in numerical simulations of interactions and or merging of galaxies (e.g., Toomre & Toomre 1972).

4. Most galaxies have companions, $\sim$ 73%, which means that most WRGs are located in rich galaxy density environments. The presence of such companions might be the cause of galaxy activity and peculiarity. Furthermore, several galaxies with companions (50% of the whole sample) show the presence of a common extended halo. These common halos are characteristic of E+E galaxy collisions or mergings.

5. About 30% of the WRGs are members of a known group or cluster of galaxies. About 10% have observed associated X-ray haloes, suggesting that part of the extended ionized gas could be enhanced by intracluster gas or by galaxy interaction with a gas-rich companion.

6. The previous results are consistent with a general scenario for radio galaxies (Heckman et al. 1986), in which the powerful sources are preferable in low density galaxy regions, while weak sources are preferable in high or moderate galaxy regions.

7. A comparison of the position angles of the optical stellar continuum and the radio synchrotron continuum shows no correlation. This result is consistent with Baum & Heckman (1989a), results for moderate redshift radio galaxies.

8. The $(V-R)$ and $(R-I)$ colors of WRGs lie in the region dominated by AGNs and below the region of normal ellipticals and the bulges of spirals. The locus of WRGs is indicative of star formation activity, AGN activity or both. Most galaxies with rather unusual colors compared to the majority of WRGs have peculiar morphology and/or galaxy companions, and these objects are more likely to have recent or ongoing star formation produced by the galaxy tidal interaction or merger.

9. The surface brightness profiles of the elliptical WRGs were divided into three groups, according to the degree of possible tidal influence by their neighbors (Kormendy 1977): Class T1, dynamically isolated, (47%); Class T2, unclear degree of tidal influence, (13%); and Class T3, galaxies which have at least one companion of comparable or greater brightness located within several diameters, (23%).

10. The peculiarities present in the elliptical WRGs produce deviations of the intensity profiles from the de Vaucouleurs law. Classes T2 and T3 show strong deviations from de Vaucouleurs law specially in the external regions of the WRGs, while the group T1 successfully reproduces the light curve of a galaxy with a de Vaucouleurs $r^{-1/4}$ law at most radii.

11. Most WRGs (83%) show an internal turnover, small bump or flatness of the brightness profile in the innermost regions, which could correspond to an additional light component in the profile (nuclear excess), as compared to normal ellipticals de Vaucouleurs type profiles.

12. The tidal effects evident in outer parts of the WRGs profiles, are consistent with Kormendy's conclusion that elliptical galaxies with nearby companions of comparable luminosity have bright envelopes above the extrapolation of a de Vaucouleurs law fitted to the inner parts, and that these envelopes are greatly reduced or absent in isolated galaxies.

The authors wish to thank an anonymous referee for helpful comments and suggestions which greatly improved the paper. We also thank L.A. Martínez for his help with the reduction software packages, the OAN/SPM team of night assistants: G. García, S. Monroy, J. Velazco and F. Montalvo, and the technical support group. R. Carrillo acknowledges the scholarships received from CONACyT and DGAPA-UNAM during his graduate studies at UNAM. This project has been partially supported by grants IN300789 and IN501694 (DGAPA, UNAM).

REFERENCES

Aceves, H., Cruz-González, I., & Carrillo, R. 1997, in preparation
Baum S.A., Heckman, T., Bridle, A., van Breugel, W., & Miley, G. 1988, ApJS, 68, 643
Baum S.A., & Heckman, T. 1989a, ApJ, 336, 681
_____. 1989b, ApJ, 336, 702
Black, A.R.S., Baum, S.A., Leahy, J.P., Perley, R.A., Riley, J.M., & Scheuer, P.A.G. 1992, MNRAS, 256, 186
Capetti, A., Morganti, R., Parma, P., & Fanti, R. 1993, A&AS, 99, 407
Carrillo, R. 1995, Ph.D. Thesis, Universidad Nacional Autónoma de México
Carrillo, R., & Martínez, L.A. 1997, Reporte Técnico, Instituto de Astronomía, UNAM, in preparation
Carrillo, R., Cruz-González, I., & Guichard, J. 1997, in preparation
Chambers, K., Miley, G., & van Breugel, W.J.M. 1987, ApJ, 327, L47
Colla, G., et al. 1973, A&AS, 11, 291
Colla, G., Fanti, C., Fanti, R., Gioia, I., Lari, C., Lequeux, J., Lucas, R., & Ulrich, M.H. 1975a, A&A, 38, 209
_____. 1975b, A&AS, 20 1
Cornell, M.E., Aaronson, M., Bothun, G., & Mould, J. 1987, ApJS, 64, 507
Cruz-González, I., Carrillo, R., & Salas, L. 1997, in preparation
de Ruiter, H.R., Parma, P., Fanti, C., & Fanti, R. 1986, A&AS, 65, 111
Fanaroff, B.L., & Riley, I.M. 1974, MNRAS, 167, 31P
Fanti, C., Fanti, R., de Ruiter, H.R., & Parma, P. 1986, A&AS, 65, 145
_____. 1987, A&AS, 69, 57
Fanti, R., Gioia, I., Lari, C., & Ulrich, M.H. 1978, A&AS, 34, 341
Fanti, R., Gioia, I., Lari, C., Lequeux, J., & Lucas, R. 1973, A&A, 24, 69
Gallagher, J.S. 1986, PASP, 98, 81
González-Serrano, J.I., & Carballo, R. 1993, AJ, 105, 1710
González-Serrano, J.I., & Pérez-Fournon, I. 1991, A&A, 249, 75
Hamuy, M., & Maza, J. 1987, A&AS, 68, 383
Heckman, T.M. 1981, ApJ, 250, L59
Heckman, T.M., Smith, E.P., Baum, S.A., van Breugel, W.J.M., Bothun, G.D., & Balick, B. 1986, ApJ, 311, 526
Jones, C., Mandel, E., Schwarz, J., Forman, W., Murray, S.S., & Harnen, Jr., F.R., 1979, ApJ, 234, L21
Kent, S.M. 1984, ApJS, 56, 105
Kormendy, J. 1977, ApJ, 218, 333.
Kotanyi, C.G. 1979, A&A, 74, 156
Kotanyi, C.G., & Ekers, R.D. 1979, A&A, 73, L1
Landolt, A.U. 1983, AJ, 88, 439
Mazzarela, J.M., & Boroson, T.A. 1993, ApJS, 85, 27
Mc Carthy, P., van Breugel, W., Spinrad, H., & Djorgovski, S. 1988, ApJ, 321, L29
Merritt, D., & de Zeeuw, T. 1983, ApJ, 267, L19
Miley, G.K., Heckman, T.M., Butcher, H., & van Breugel, W.J.M. 1981, ApJ, 247, L5
Moles, M., García-Pelayo, J.M., Masegosa, J., Aparicio, A., & Quintana, J.M. 1985, A&A, 152, 271
Morganti, R., Fanti, C., Fanti, R. Parma, P., & de Ruiter, H.R. 1987, A&A, 183, 203
O'Dea, C.P., Gallimore, J.F., & Baum, S.A. 1995, AJ, 109, 26
Parma, P., de Ruiter, H.R., Fanti, C., & Fanti, R. 1986, A&AS, 64, 135
Parma, P., Fanti, C., Fanti, R., Morganti, R., & de Ruiter, H.R. 1987, A&A, 181, 244
Poulin, P. 1988, A&AS, 72, 215
Quinn, P.J. 1984, ApJ, 279, 596
_____. 1989, in ESO Workshop on Extranuclear Activity in Galaxies, ed. E.J.A. Meur & R.A.E. Fosbury, ESO Conf. and Workshop Proc. No. 32, 347
Quinn, P.J., & Herquist, L. 1987, in IAU Symp. 107, Structure and Dynamics of Elliptical Galaxies, ed. T. de Zeeuw, (Dordrecht: Reidel), 249)
Savage, B.D., & Mathis, J.S. 1979, ARA&A, 17, 73
Schuster, W.J. 1982, RevMexAA, 5, 149
Simon, A.J.B. 1979, MNRAS, 188, 637
Smith, E.P., & Heckman, T.M. 1989a, ApJS, 69, 365
_____. 1989b, ApJ, 341, 658
Toomre, A. 1977, in The Evolution of Galaxies and Stellar Populations, ed. B.M. Tinsley & R.B. Larson, R.B (New Haven: Yale Univ. Observatory), 401
Toomre, A., & Toomre, J. 1972, ApJ, 178, 623
Ulrich, M.-H., Kinman, T.D., Lynds, C.R., Rieke, G.H., & Ekers, R.D. 1975, ApJ, 198, 261
van Breugel, W., Heckman, T., & Miley, G. 1984, ApJ, 276, 79
Whitford, A.E. 1971, ApJ, 169, 215

René Carrillo and Irene Cruz-González: Instituto de Astronomía, UNAM, Apartado Postal 70-264, 04510 México, D.F., México. (rene@astroscu.unam.mx).
José Guichard: Instituto Nacional de Astrofísica, Optica y Electrónica, Apartado Postal 216, 72000 Puebla, Pue., México.